PRINCETON UNIVERSITY OBSERVATORY
Princeton, New Jersey 08544

FINAL PROJECT REPORT

for NASA Grant
NSG-7618

Photon Counting Image Sensor Development for Astronomical Applications

Covering the Period
July 1, 1979 to September 14, 1987

Submitted to:

HEADQUARTERS
NATIONAL AERONAUTICS AND SPACE ADMINISTRATION
Washington, DC 20546

By: Edward B. Jenkins
Edward B. Jenkins
Principal Investigator
Princeton University Observatory
Princeton, N. J. 08544
Tel: 609-452-3826

November 15, 1987

1. Background

In the mid 1970's, Princeton's Department of Astrophysical Sciences was very active in developing 2-dimensional imaging devices which would operate at ultraviolet wavelengths. This effort was a natural outgrowth of the heritage of developing and using the telescope and spectrometer which flew on the *Copernicus* satellite. In addition, we had a keen interest in contributing to the technological steps needed for instruments which were to fly on the Hubble Space Telescope (then called the Large Space Telescope).

In our efforts to develop the SEC vidicon for Princeton's proposed Wide Field Camera on the Space Telescope, we were conscious of the limitations on quantum efficiency which were inherent with semi-transparent photocathodes. Research by G. Carruthers at NRL emphasized that opaque photocathodes on a smooth substrate provided excellent quantum efficiencies ($\sim$ 70%, as opposed to around 15 - 20% for the semi-transparent ones). Moreover, with an opaque photocathode where the electrons are emitted from the front side of the illuminated surface, one could operate with a windowless configuration. This feature allowed the registration of ultraviolet fluxes below the transmission cutoff of even the best uv optical materials, such as MgF_2 or LiF. From our experience with *Copernicus*, we had a special insight on the scientific importance of doing spectroscopy within the interval from the Lyman limit up to a wavelength of around 1150Å.

Our earliest thoughts (around 1975) were to experiment with a detector where electrons bombarded a self-scanned CCD-type silicon diode array target. The electro-optical arrangement was to consist of a focusing magnetic field which was inclined to the opposing photocathode and detector element surfaces, so that the photoelectrons could be deflected away from the incident optical beam as they were accelerated by a strong $\vec{E}$ field. As an initial step, under the sponsorship of Princeton's Plasma Physics Laboratory we obtained some experience in working with electron-bombarded CCDs in electrostatically focussed image tubes. Our task at the time was to supply a large-area, sensitive image sensor for their fusion research program.

2. Initial Program Objectives

In 1978 NASA expressed an interest in supporting research and development for new detectors which could be used in future uv astronomy missions in space. In response to this initiative, we submitted a proposal in July of that year to purchase some specially built intensified CCD (ICCD) detector tubes from Varian and investigate the performance of the electron bombardment process. In addition to studying the signal characteristics of the photoevents, we were particularly interested in demonstrating that back-illuminated chips were not susceptible to radiation damage to their clocking electrodes. It was known at that time that other investigators had found serious degradation in the performance of CCDs bombarded on their front sides.

3. Early Conclusions on Electron-Bombarded CCDs

In the year which followed, we investigated the response of a thinned, back-illuminated CCD to bombardment by 20 keV electrons. The CCD was manufactured by Texas Instruments (TI), had 160 $\times$ 100 pixels, and was enclosed in a sealed tube manufactured by Varian. The CCD was cooled to a low temperature so that long integration and readout times could be used to give the best amplifier performance within reasonable bandwidth constraints. Examples of typical events and a pulse height distribution were shown in an article by Lowrance, *et al* [ref. 1].

We followed the research on the TI CCD by concentrating on a very promising new CCD design developed by RCA. As it turned out in years which followed, this CCD was the centerpiece of our ICCD research efforts and was eventually adopted as the CCD which was used by Princeton's IMAPS sounding rocket payload (see §**6** below). In the earliest efforts with the RCA chip, we collaborated with CCD development engineers at RCA to develop improved circuit designs (both on and off chip) for low-noise readout of their CCDs at slow scan rates. As an outgrowth of these activities, we learned much about how to optimize the operation of their devices, and they, in turn, were motivated to improve the design of their on-chip amplifiers to

increase the signal-to-noise ratio. Indeed, their next generation of CCDs of the same variety showed a noticeable improvement in performance over the earlier devices.

Once we had made some progress in working with the RCA CCDs, we embarked on a program to evaluate the response of their back-illuminated, thinned chips to very energetic electrons. We installed a CCD in a demountable arrangement consisting of an oblique-focus ITT image section (developed under support from a NASA grant to J. Williams at GSFC) located in a permanent magnet focus assembly provided by G. Carruthers at NRL. Electrons from the opaque CsI photocathode were accelerated onto the CCD by electric fields ranging from 3 to 26 kV. As with the earlier tests using the TI CCD, the RCA CCD was operated in a slow scan mode and cooled to $\sim$-100 ° C.

Figure 1 shows the pulse height distributions which were obtained at different accelerating voltages. For the first time, we obtained a clear indication that the main peak was easily separable from low-level noise events at accelerating voltages above about 15 kV. However, some events of intermediate amplitude were detected away from the main photoevent peak. After further tests were made, Zucchino, *et al.* [ref. 5] gave a summary of the conclusions from the ICCD development efforts. This article described the newer, two-stage, low-capacitance amplifiers on the RCA chips and gave the results of measurements of their amplifier gains and readout noise levels. The article gave evaluations of the secondary electron yield *vs.* incident electron energy and surveyed the problem of the "dead layer" which resulted in a threshold energy for the linear yield trend (see, e.g. Figure 2 in this report -- for the CCD characterized here, the dead layer robs 7.5 kV worth of incident energy. The offset varies substantially from one CCD to another for reasons which are poorly understood). A brief discussion of charge transfer measurements at different locations and the sensitivity of the CCD to 6 keV x-rays was also presented. A serendipidous discovery that the on-chip amplifier emits light and can thus add on an uneven background was discussed in a separate article by Zucchino, *et al.* [ref. 3].

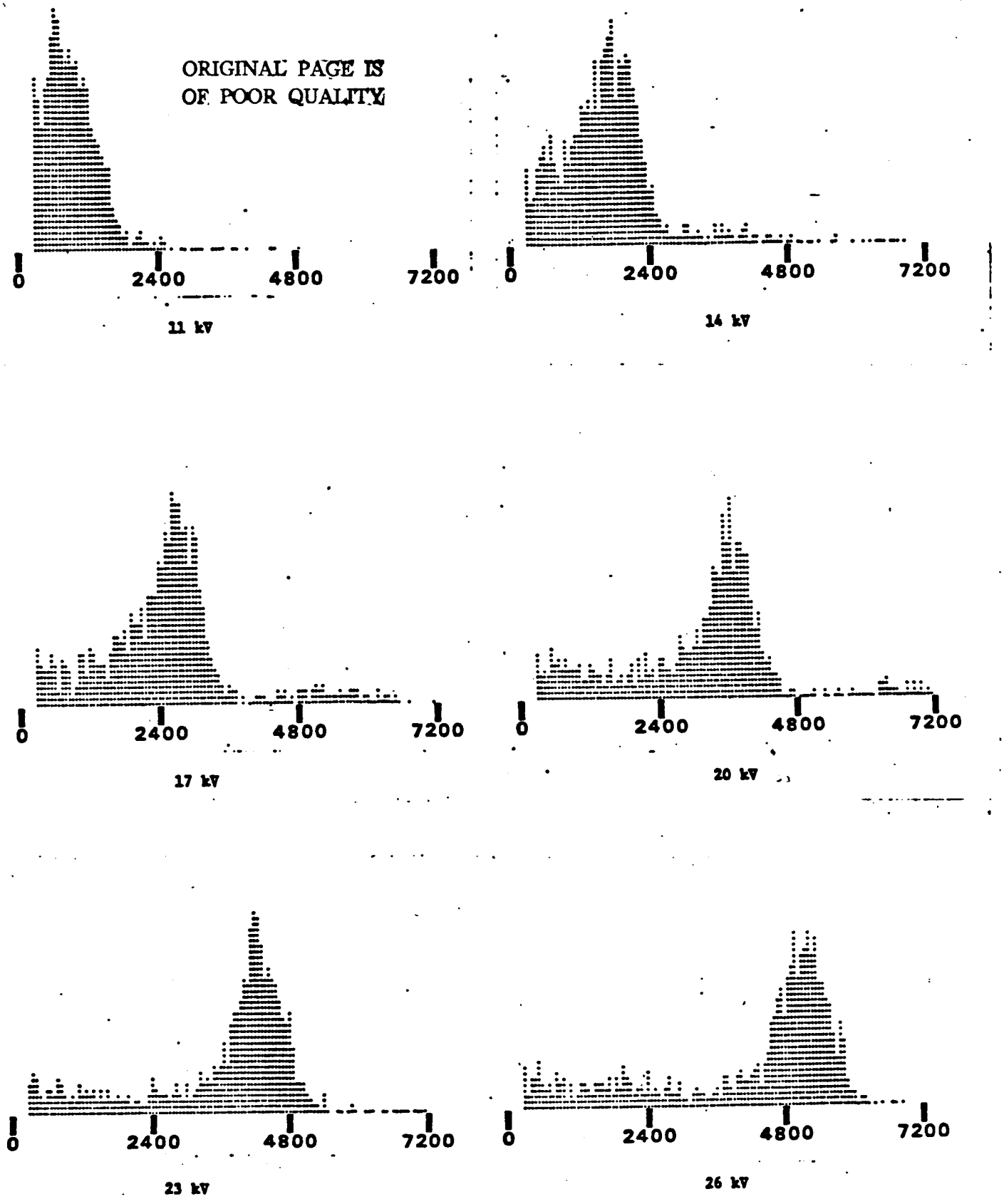

Figure 1. Pulse height distributions for the total charge generated by energetic electrons as they impact Si layer of an RCA CCD. The different plots show the behavior for various accelerating voltages for the electrons.

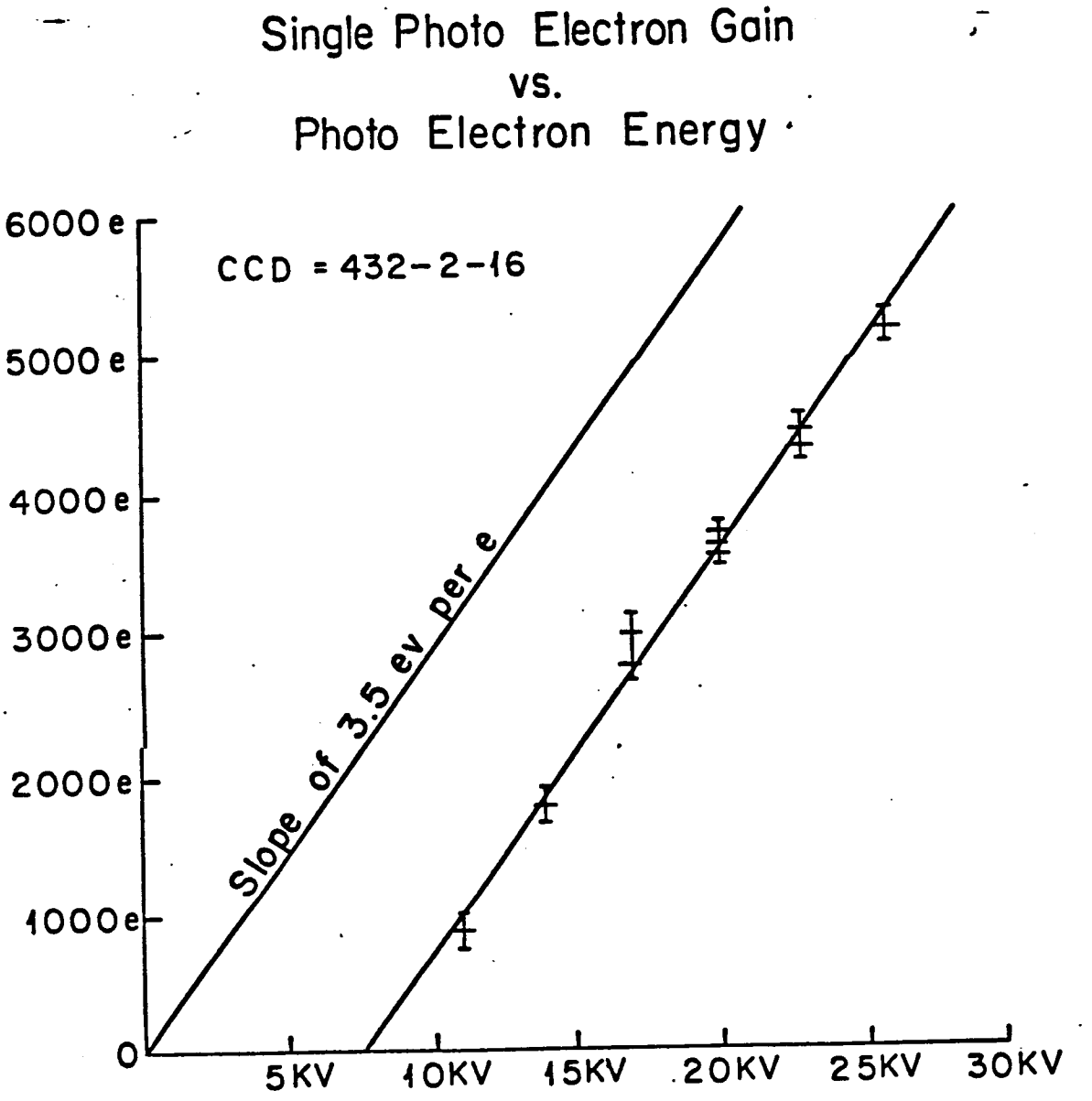

Figure 2. Modal gain for generating secondary electrons as a function of accelerating voltage. The displacement of the trend away from the plot's origin is caused by the energy consumed by the CCD's dead layer.

In addition to our experiments on the electron bombardment of RCA CCDs, we also tested several thinned, virtual phase CCDs manufactured by Texas Instruments and purchased by GSFC. For the best of these devices, the yield of 2100 secondary electrons per incident primary at 20 kV was not as good as that of the RCA CCD, where we obtained approximately 3600 electrons at the same accelerating voltage (see Fig. 2). An important result from the tests with the virtual phase CCD was that no substantive damage was caused by having a large dose of enegertic electron impacts on the front side. The only effect found by Everett, [ref. 7] was a change in the clocking potentials which were required for good charge transfer efficiency.

4. Research on Event Centroiding

4.1. Early Developments

From our early investigations, it was clear that for many photoevents recorded by the CCD not all of the secondary charges were deposited in a single pixel (see Fig. 8 of ref. 1). For sure, the secondary electrons are generated within the first few microns of the silicon behind the dead layer. However, as the electrons diffuse across the remaining silicon toward the charge collection sites, they spread laterally, and for events somewhat displaced from the center of a pixel the expanding charge cloud is eventually partitioned into more than one potential well defined by the voltages on the clocking electrodes. Thus, as a rule, photoevents generate multiple signals in adjacent pixels. We were interested in evaluating whether or not one could compare these signal amplitudes and determine with some precision where the incident electron landed relative to the pixel boundaries. It occurred to us that processing information on the charge configuration of individual events might ultimately enable the detector to yield a finer spatial resolution than the size of the CCD pixels. Appendix A, taken from one of our proposals for this grant research, describes how to perform the centroid analysis for a 2-dimensional Gaussian distribution of charge (the true distribution is closer to being an exponential; see §**4.2**).

To determine quantitatively how much positional accuracy could be achieved in principle, we performed a Monte-Carlo computer simulation of how solutions for the event locations would be affected by signals in the presence of noise. We assumed that the distribution of secondary electrons corresponded to the point spread function for blue light excitation of a 15μ thick CCD, since the blue light has an absorption depth comparable to the range of 20 keV electrons in silicon.

Figure 3 shows the image which we synthesized from the simulation of a 5×5 checkerboard illumination pattern within a single 25μ pixel. In this case, the total charge from each photoelectron event corresponded to 50 times the rms noise in a single CCD pixel, which seemed to be a realistically achievable value in slow-scan applications. One can see that the individual 5μ squares are resolved.

The Monte-Carlo program for event simulation and analysis was also used to investigate how the response to the checkerboard pattern varied as a function of signal-to-noise ratio. In addition, we used a pattern of 5μ wide bars in the computer simulation to derive the square-wave amplitude response (SWAR) at 100 line pairs mm^{-1}. Figure 4 shows the representative SWAR and checkerboard responses. A third curve shows the rms error in the calculated positions of the photoelectrons. A further conclusion from the simulation was that one could employ somewhat incorrect assumptions on the width of the spread function in the analysis and still achieve satisfactory results for the events' centroid locations.

One could be critical of the computer simulations since they modeled an idealized situation where the CCD response was locally uniform and the distribution function for the electrons was constant. The degree to which these conditions would be satisfied with real CCDs and the magnitude of various intangible sources of uncertainty were phenomena which were important to investigate, however. An important intermediate step, however, was to determine the *average* properties of the spread functions. Appendix B discusses how to measure the projection (along rows or columns) of the average charge spread profile.

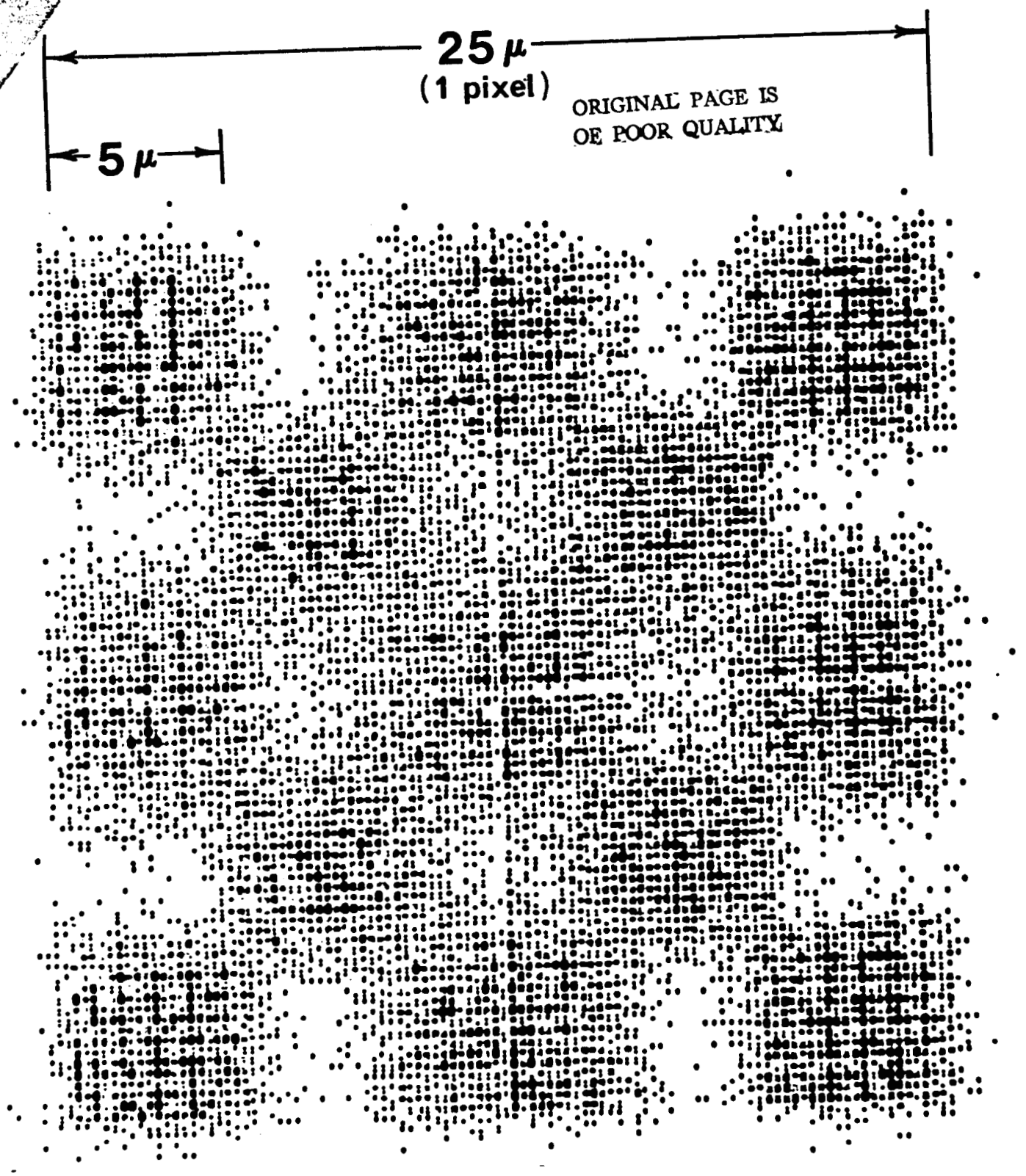

Fig. 3 - Subpixel pattern detail obtained from the analysis of charge amplitudes in adjacent pixels. In a computer simulation, we calculated the signals from many photoelectron hits in a checkerboard pattern, added random numbers to the signals, and then solved for the most likely positions of hits. Different darknesses in the figure correspond to different densities for the reconstructed events. The noise amplitudes had a Gaussian distribution with an amplitude of 1/50 times that of the number of secondary electrons in a single hit.

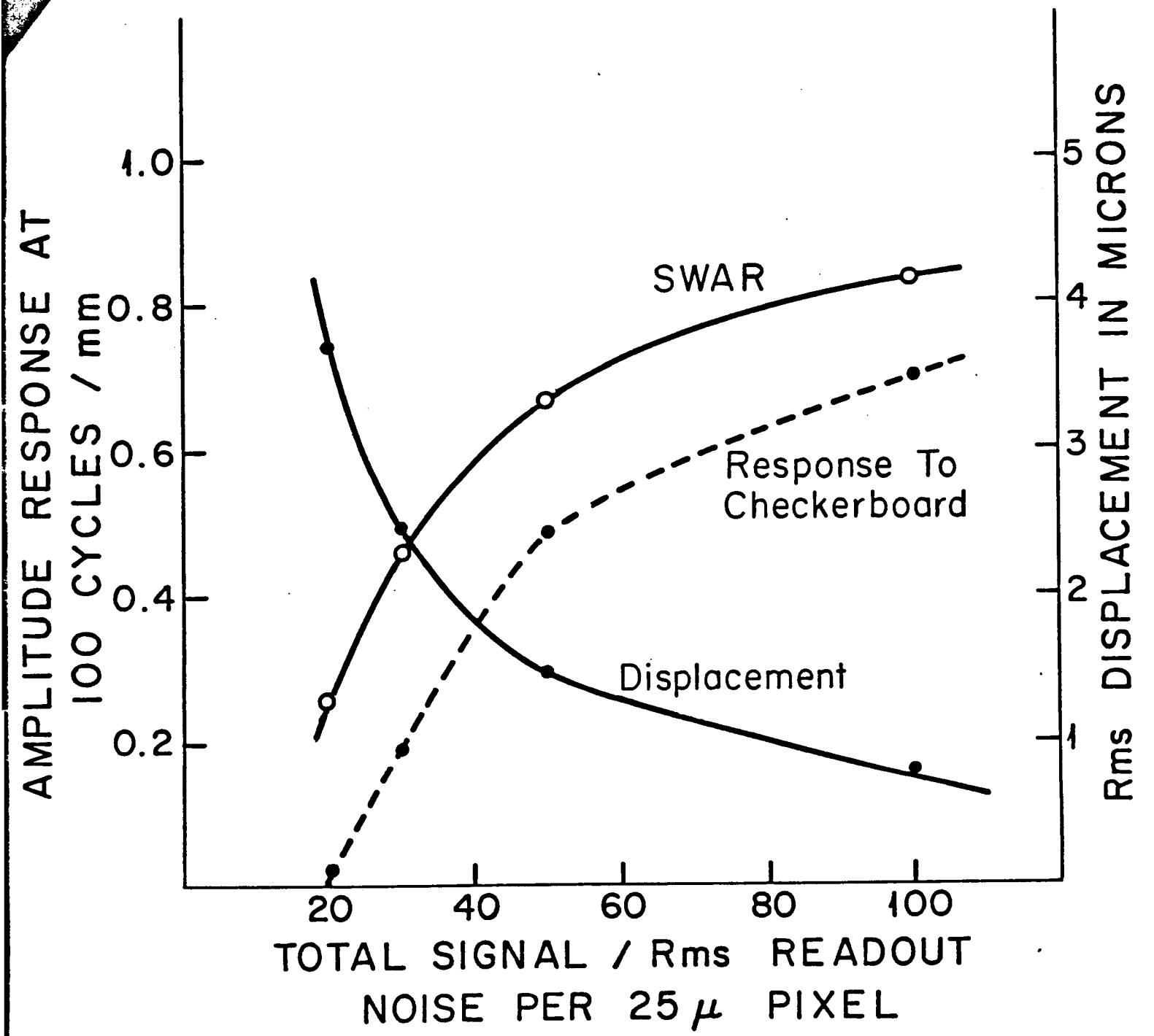

Fig. 4 - Resolution performance expected from the pixel charge analysis as a function of signal-to-noise ratio. From simulations similar to that which is shown in Fig. 3, we calculated the amplitude response to one-dimensional square waves (i.e., bars) - shown by the curve labeled SWAR, the response to checkerboard squares, and the rms positional error of hits- shown by the curve labeled displacement.

We wrote a computer program to identify discrete photoevents in areas of the image format where the event rates were low enough that there would be little confusion from chance overlaps. The program recognized photoevents by scanning for pixels which exceeded a certain threshold (well above the readout noise) in frames where the CCD fixed pattern background had been removed. Once this threshold had been passed, the total charge collected in a 3×3 box centered on the hot pixel was measured. Care was taken to insure that events were not counted twice when more than one pixel exceeded the threshold in a small area. Also, events which might be contaminated by a nearby event were rejected. For valid, clean events, we measured and stored values of the fractional charges along columns and rows.

On the basis of extensive tests with the RCA CCD operated in slow-scan mode in the demountable, oblique-focus image section, we used the analysis program described above to determine that the projection of the spread function convolved with a CCD pixel (see the figure in Appendix B) closely approximated the relation:

$$F(y_0) = 0.455 \exp[-y_0/(0.135 \text{ pixel})] + 0.02$$

The characteristic width of this function, in our opinion, was close to ideal for our goal of accurate event centroiding. Narrower events would be lost inside a single pixel for hits reasonably near the center, while broader events would have decreased overall centroiding accuracy because they'd be too diffuse.

Some actual attempts to centroid with a real image registered by an ICCD were performed under support of another NASA grant (NSG-5277) to Princeton. Figure 5 shows that indeed one could obtain a sharper image than expected if one had integrated the analog charges in the pixel bins. This test was performed in 1981, and we felt that its outcome was limited more by our inability to obtain a sharp optical focus rather than our capability to centroid events accurately.

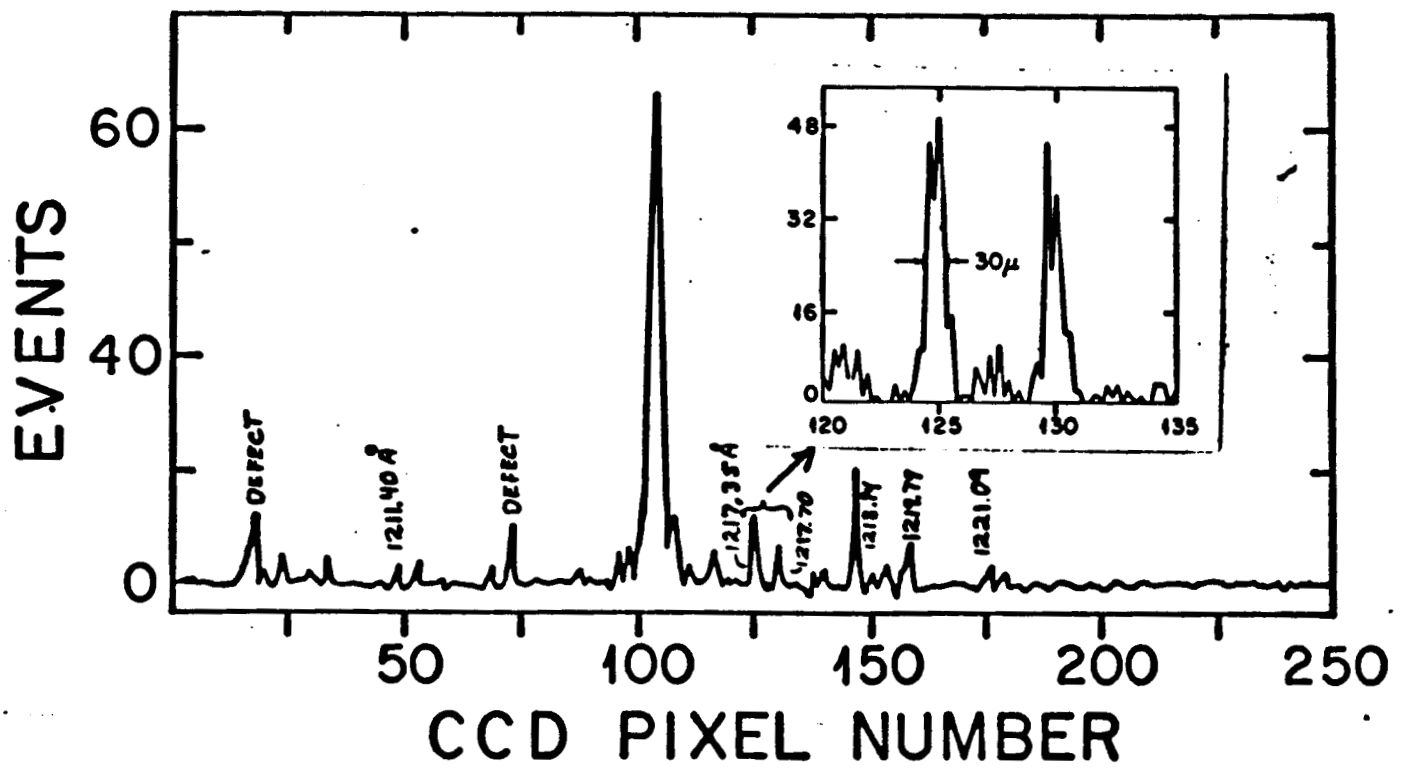

Figure 5. Spectrum of a molecular hydrogen lamp taken with an oblique, off-axis focusing ICCD on August 24, 1981. The strong line is L-α emission from atomic hydrogen. The inset shows an expanded section of a longer exposure fo the same spectrum. Discrete events were identified, had their centroid positions calculated, and then accumulated in computer memory bins at 6μ resolution.

4.2. Recent Results

Further attempts to test how well we could centroid photoevents with an ICCD were not carried out until 1986 and 1987, mostly under support from a currently active NASA grant to design, build and fly the *Interstellar Medium Absorption Profile Spectrograph* (IMAPS) for sounding-rocket missions. It is relevant to discuss the results here, since the effort to build a detector for this payload was supported by the ground work in this detector development grant (see §6 below). Furthermore, the more refined efforts to investigate charge spreading and centroiding performance were a follow-on to the work started here.

As described in Appendix B, we bathed the photocathode with a uniform illumination of ultraviolet light, so that the positions of impacts would be randomly distributed with respect to the pixel boundaries. After isolated events in the readout signal were identified, we measured the fractional charges accumulated in either rows or columns. We performed these measurements for two experimental cases: (1) events registered during a rocket flight with one particular CCD installed and (2) laboratory operation of the detector with a different CCD (but of the same variety -- an RCA type 501 CCD).

Figure 6 shows the histogram of fractional charges accumulated along rows during the rocket flight. (We could not measure reliably the column charges, due to difficulties in obtaining an absolutely clean separation of signals from adjacent pixels along any given row. The problem was caused by some mild instabilities in line synchronization when the analog signals were being digitized for computer processing.) An identical presentation for the output from the laboratory tests is shown in Fig. 7. The difference in the distributions can be attributed to slight differences in the lateral spread of secondary electrons from one CCD to another. Compared to the CCD flown in the rocket, the one tested in the laboratory setup had a somewhat greater breadth for its photoevents. While we have data for only two CCDs, the variation we see is probably a fair indication of changes we may expect to find from one device to another.

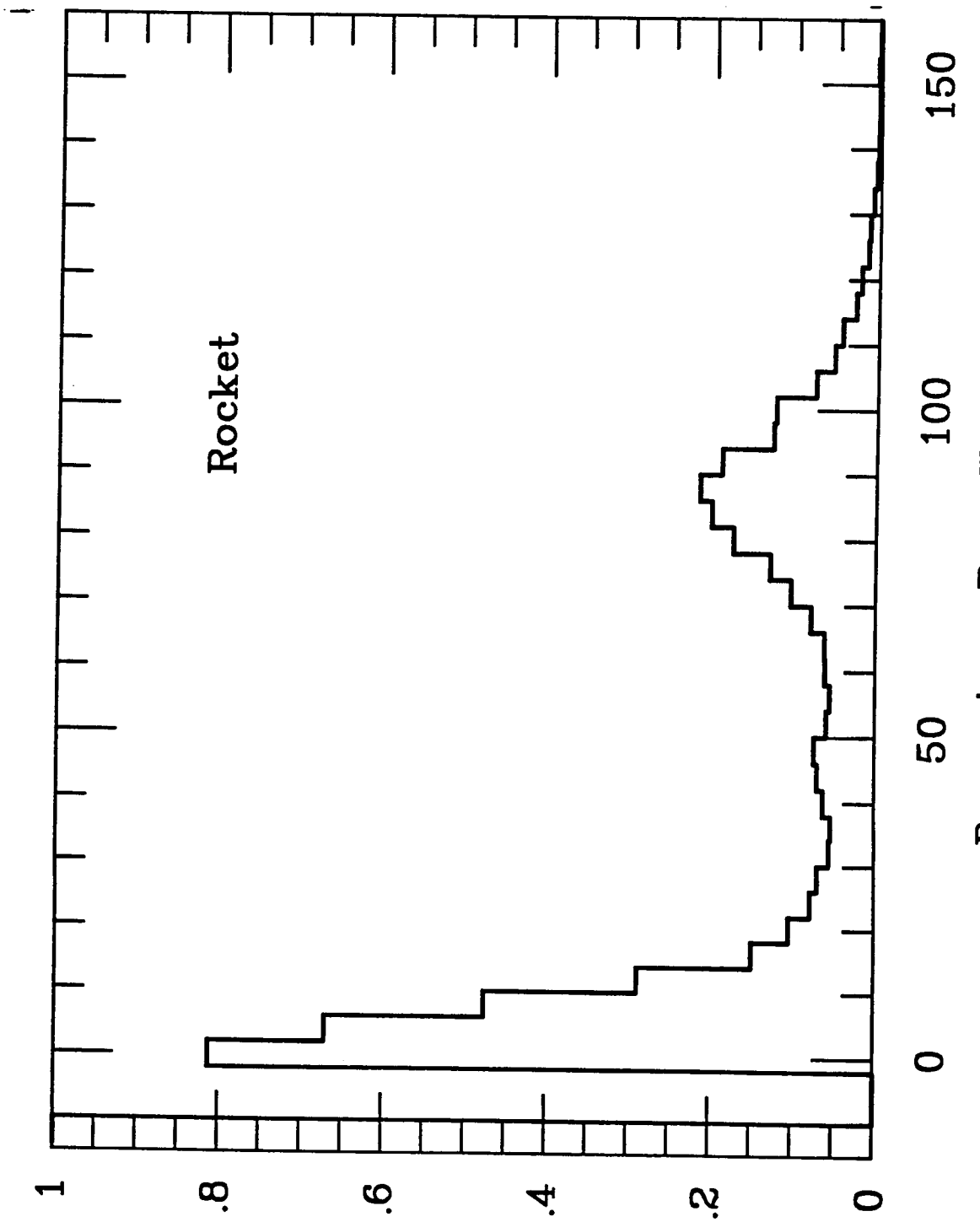

Figure 6. A histogram of event charge amplitudes, integrated along single rows, divided by the respective event's total charge. See Appendix B for a discussion of how to interpret these results. These measurements were taken from data telemetered to ground from the IMAPS payload while it observed the far-uv spectrum of π Sco.

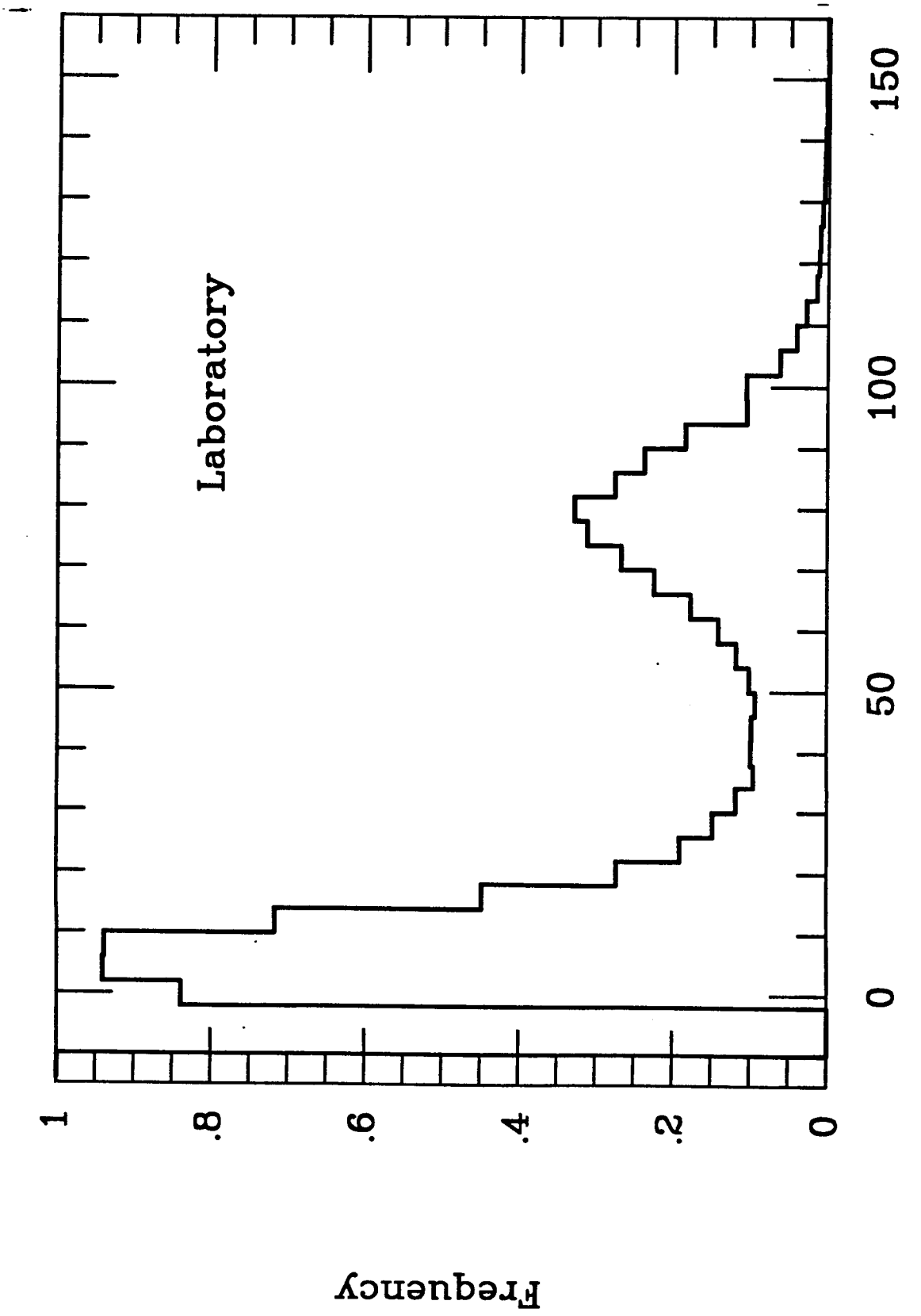

Figure 7. Same as Fig. 6, except for the CCD installed when laboratory measurements were made.

Figure 8 shows the relative amplitudes along columns for the laboratory CCD measurements. The fact that this histogram is virtually identical to the one shown in Fig. 7 demonstrates that the charge spreading is isotropic.

The charge spread function for the flight CCD is very similar to the function given by the equation in §**4.1** above. For the CCD tested in the laboratory, we found that the scale length was about 0.20 pixels instead of 0.135 pixels. Figures 9 and 10 illustrate the "buckshot patterns" for the inferred 2-dimensional structure of the electrons, just prior to their being separated and redistributed within the potential wells. The larger spread for the laboratory CCD is actually slightly more favorable for centroiding, because a photoevent which hits the center of a pixel doesn't have all of its charge lost entirely within the pixel with no spillover to reveal slight departures from the center. This fact is illustrated in Figure 11 which gives calculated rms errors σ_x in one dimension for the inferred positions, assuming the ratio of an event's total charge Q to the readout noise in a single pixel σ_r is 25. Charge distributions which straddle pixel boundaries are the most accurately located, and the error increases when the spillover charge decreases as the electron cloud gets closer to a pixel's center.

The projections for centroiding accuracies given in Fig. 11 contain an important assumption which has not yet been fully validated. We assume that the only perturbing influence in a solution for the center is the detector's readout noise. However, we do not have a full picture of how much irregularity there may be in reality for the spread functions of individual events. As presented here, our predictions take no account of the fact that the events are not of uniform size (see the paragraph below), or alternatively, that they might manifest themselves as very irregular blobs which could change in an unpredictable fashion. Ultimately, we will be able to discern the importance of the irregularities when more careful considerations are given to the goodness of fit of individual events to the average distribution (i.e., by measuring the χ^2 values and comparing them to the expected distribution function for pure readout noise).

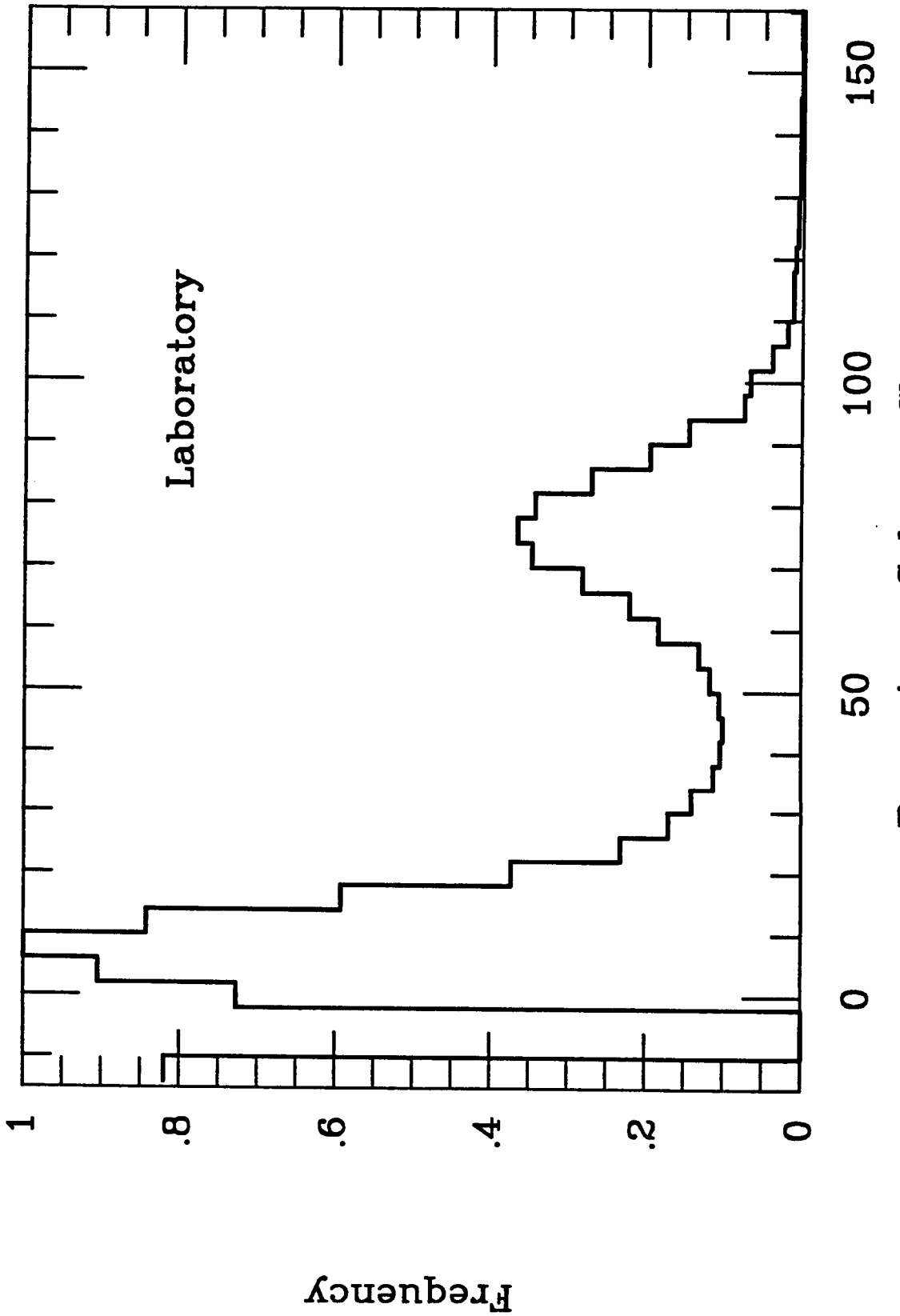

Figure 8. Same as Fig. 7, except the charge amplitudes were integrated along individual columns instead of rows.

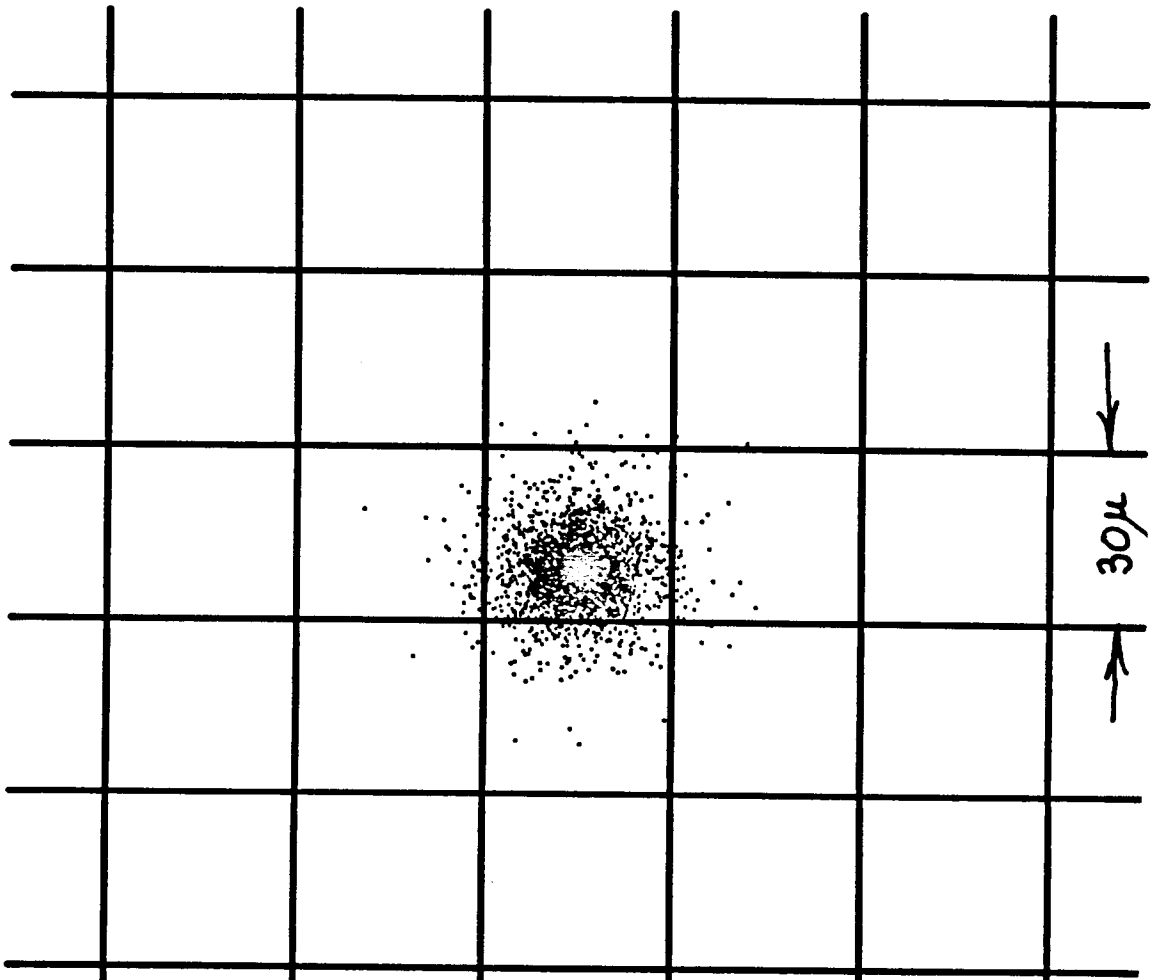

Figure 9. A reconstruction of the distribution of secondary electrons before they are segregated into the pixel cells whose borders are depicted by horizontal and vertical lines. The distribution function is inferred from the analysis (see Appendix B) of the histogram shown in Fig. 6 for the CCD on the rocket flight. The number of dots shown here corresponds approximately to the number of electrons in a typical event.

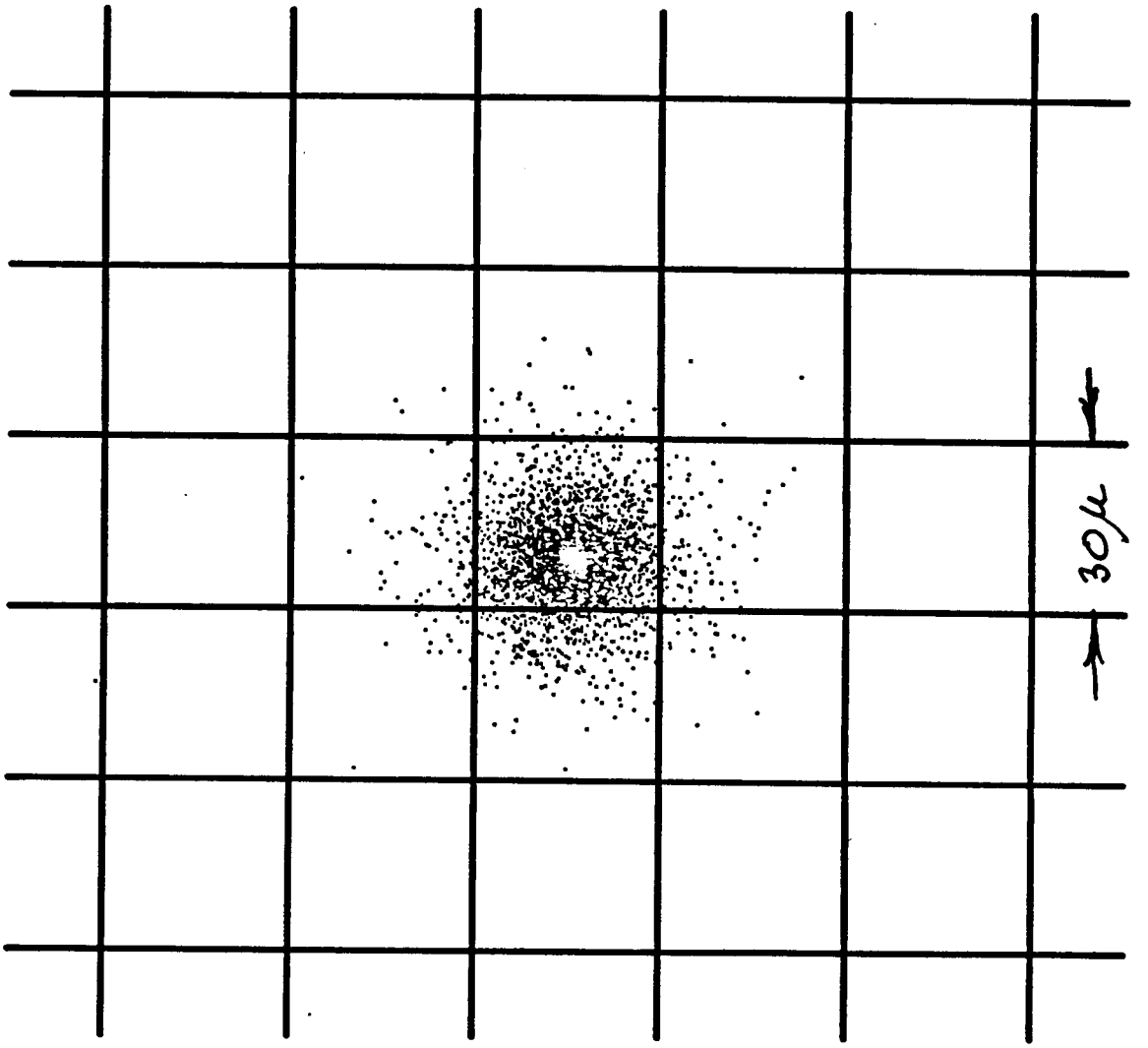

Figure 10. Same as Fig. 9, except that the distribution applies to the results from the CCD tested in the laboratory setup.

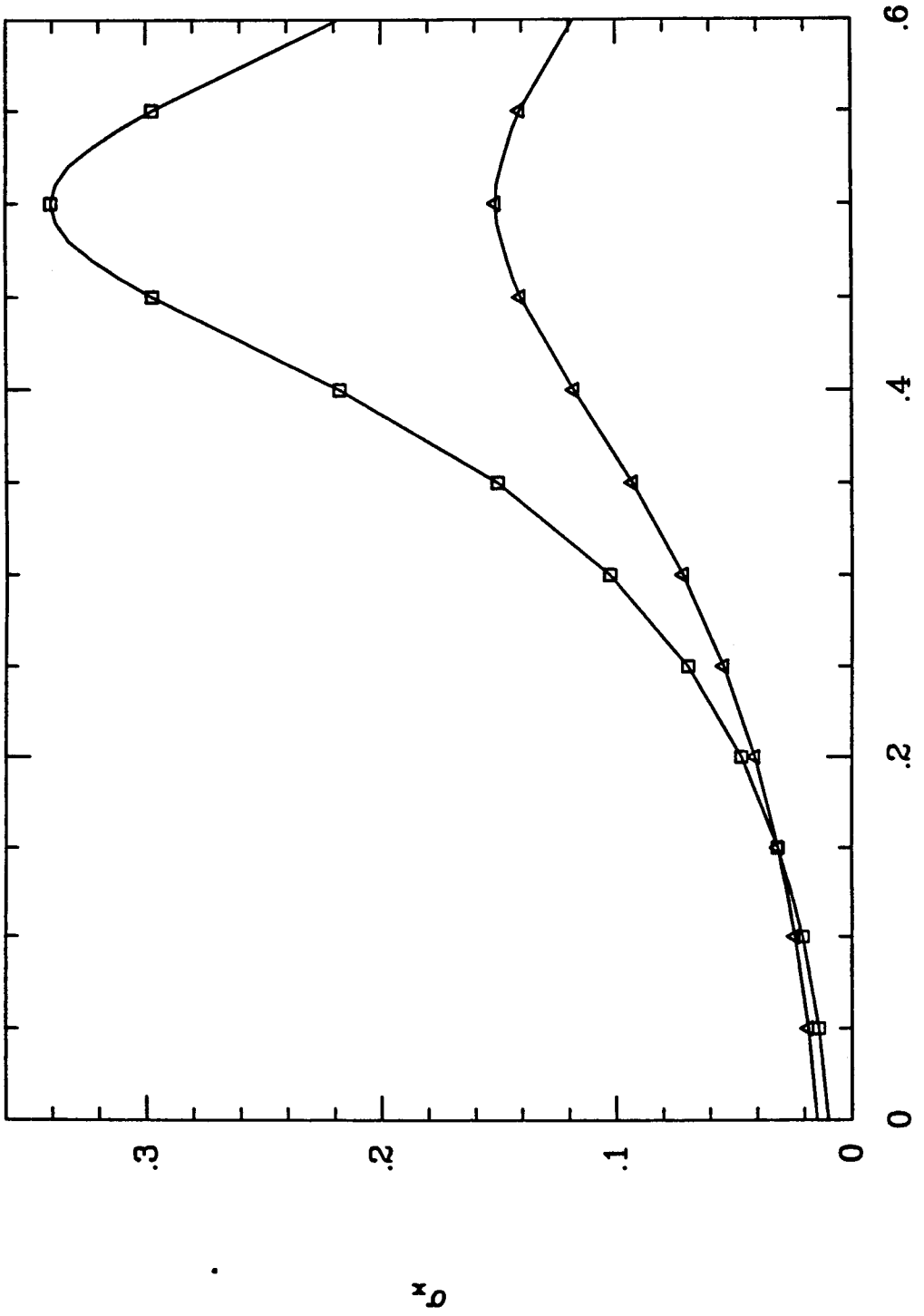

Figure 11. Computed accuracies for event locations σ_x (in one dimension), as a function of the event's distance from the edge of a pixel. The unit for σ_x is expressed in terms of the length of a pixel. Squares designate the curve applicable to the charge cloud length scale of 0.135 pixel (rocket CCD), and the triangles identify the curve for the scale of 0.200 pixel (laboratory CCD).

One interesting experiment we performed was to divide the events into two classes, according to the total charge amplitudes. Histograms for column charge distributions of events whose total charges were below and above the median are shown in Figures 12 and 13, respectively. The "more energetic events" (i.e., those with greater charge deposited in the CCD) seem to have a greater fraction of their charge thrown into adjacent pixels. The reason for this effect is not clear. Perhaps the greater mutual repulsion of the electrons is responsible for the increased spread as they migrate toward the wells.

Ultimately, the decisive test on how successfully one can centroid is to show actual results. As with the earlier experiment discussed at the end of §4.1, the most difficult part of the test is being sure the image of electrons on the CCD is sharp. A later test using a photocathode with a shadow evaporation of CsI with an Air Force Test Pattern circumvents the difficulty of obtaining a good optical focus, but the correct accelerating voltage for good electron focus can only be determined by trial and error. Figures 14 and 15 show comparisons of analog accumulations of the test pattern picture (i.e., no centroiding) and an image reconstructed from the centroid analysis of events (using an algorithm similar to the one discussed in Appendix A, but for an exponential distribution instead of a Gaussian). The main limitation in quality of the picture in Fig. 15 is probably due to the finite number of events and the associated fluctuations caused by statistical errors. In the future, we plan to repeat the test with a more efficient means for recording frames (using a special, high-speed digital recorder purchased for the sounding-rocket effort). This improvement will allow us to obtain, without an extraordinary amount of work, far more than the 4200 frames used to construct the image in the figure.

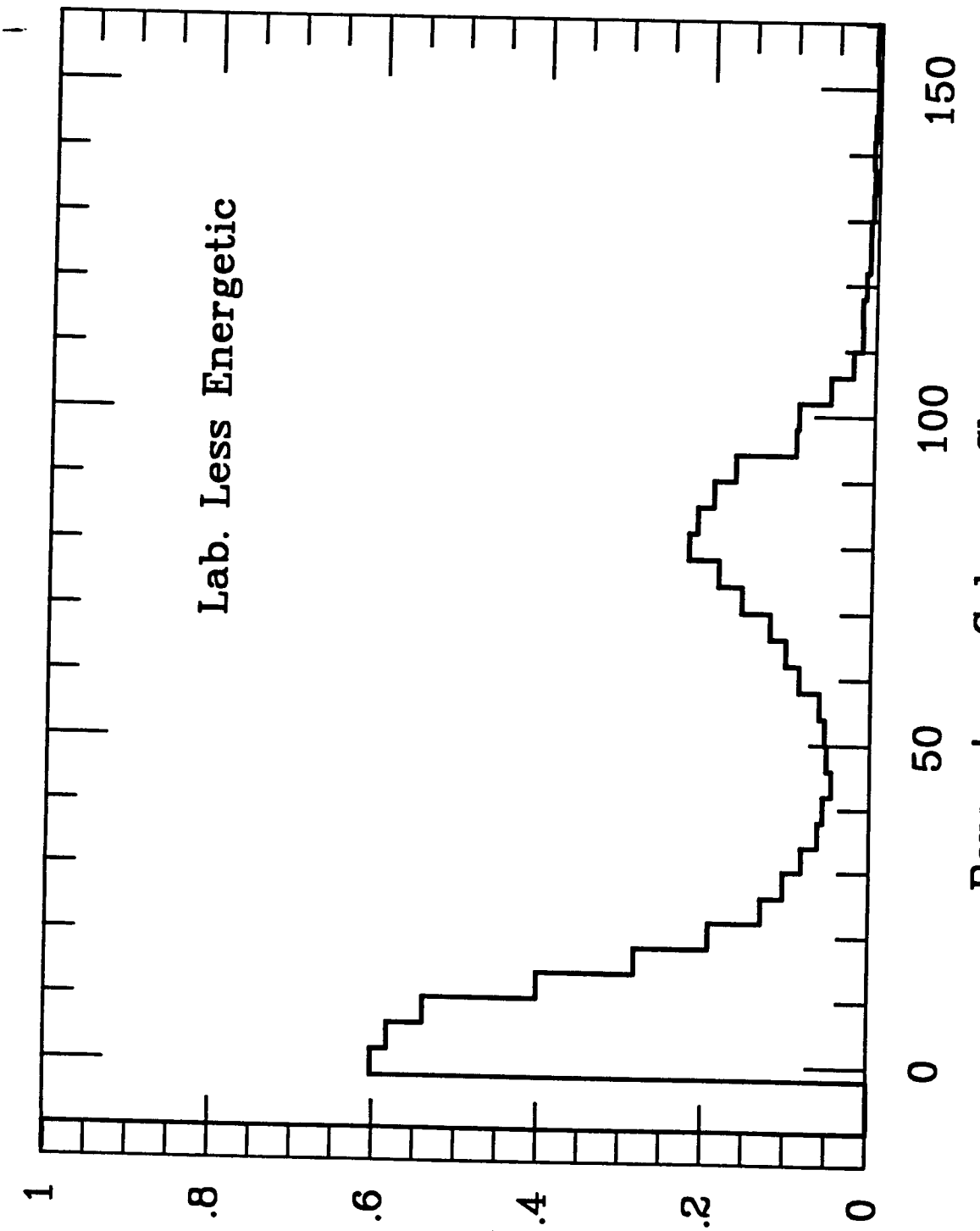

Figure 12. The distribution of percentage column charge for events whose total charge is less than the median charge Q_m.

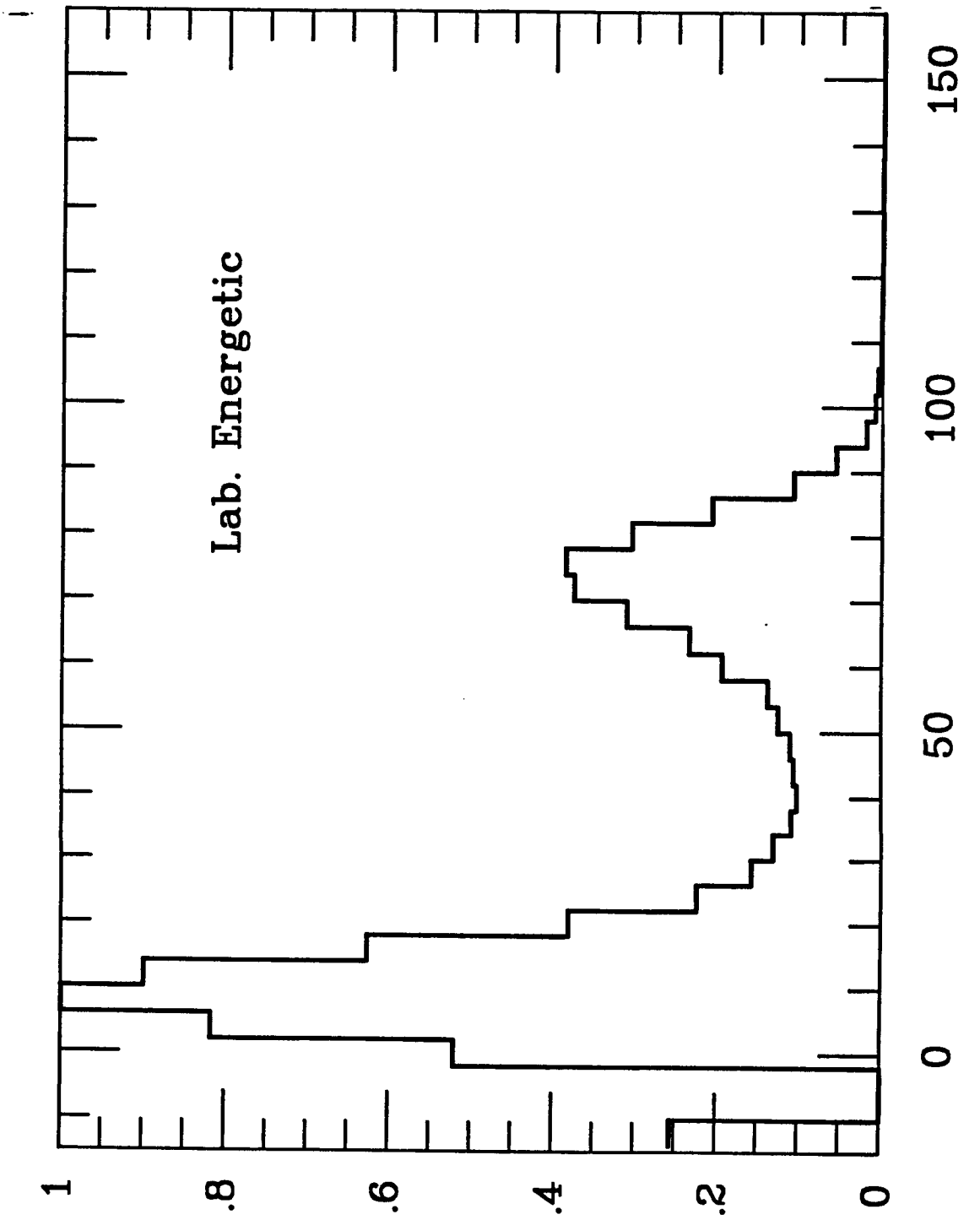

Figure 13. The distribution of percentage column charge for events whose total charge is greater than the median charge Q_m.

Figure 14. Presentation of 2400 co-added analog readouts of ICCD exposures, using a photocathode created by a shadow evaporation through a mask with an Air Force test chart pattern. The cathode was uniformly illuminated and the image pattern results from the change in quantum efficiency between the CsI and the bare, metallic substrate. Note the uneven appearance of the bars caused by the discrete binning in the CCD pixels.

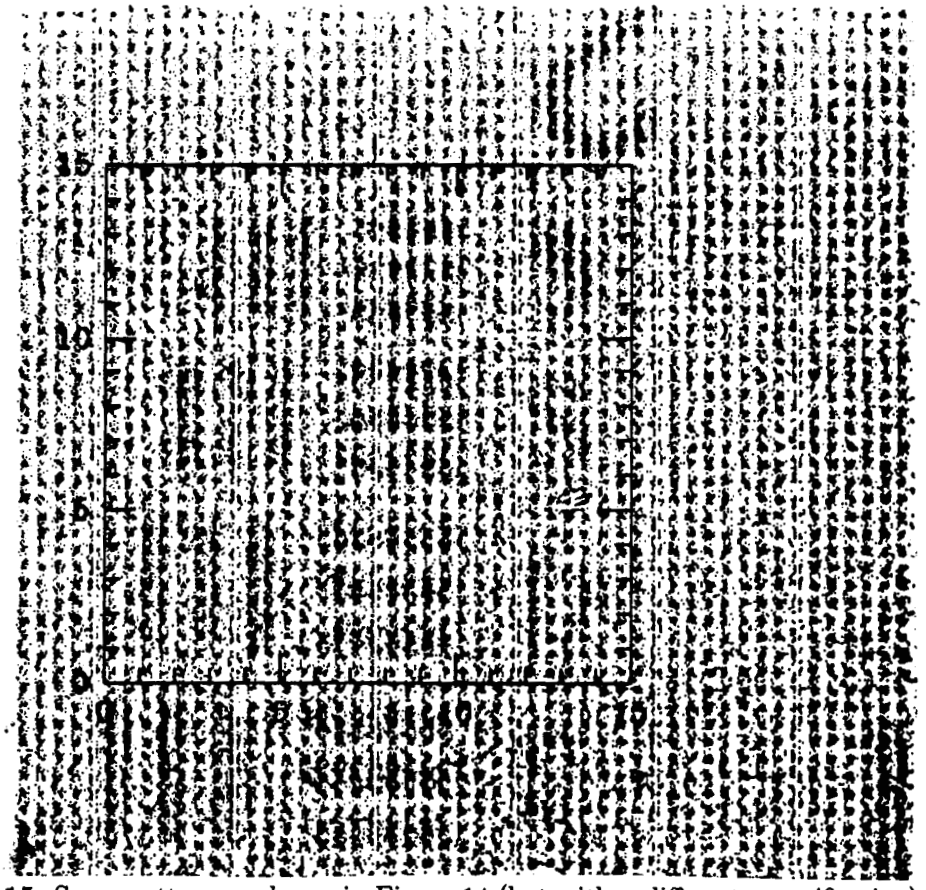

Figure 15. Same pattern as shown in Figure 14 (but with a different magnification), except that individual photoevents were identified and had their locations defined to a scale finer than the pixel size. 4200 frames were combined to produce this picture. In contrast to Figure 14, the bars are uniform. The narrow stripes are caused by some systematic problems with the signal sampling and are not intrinsic to the detector. Tick marks inscribed in the box indicate the linear scale, in units of a 30μ pixel.

5. Charge Amplitude Distribution

With the refinements in the CCDs and off-chip video sampling and amplification circuitry we achieved over several years (especially for rapid frame rates -- see §**6.7**), near the end of this grant period we were able to obtain some improvement in the isolation of charge amplitudes than indicated by distributions in Figure 1. Figures 16 and 17 show the distributions for the "Rocket CCD" and "Laboratory CCD" discussed in §**4.2** above.

The ratios of the widths of the peaks shown in the two figures to their respective median charges have important implications for the quality of an image gathered by analog accumulations of signals. When one counts the photoevents, the signal-to-noise ratio in the picture is limited only by the statistical accuracy for some finite number of events accumulated, apart from errors caused by occasional accidental detections or missed events. However, when one substitutes analog signal amplitudes for the strict numerical event reporting, the dispersion of charges deposited from one event to another adds a new source of uncertainty in the registration of integrated light intensity. In principle, this effect could be a significant source of noise above the normal, inevitable Poisson counting fluctuations. However, the analysis below shows that the effect should be hardly noticeable for the ICCD. Indeed, the main drawback in analog integrations is the compounding of readout noise over the many frames which are added together.

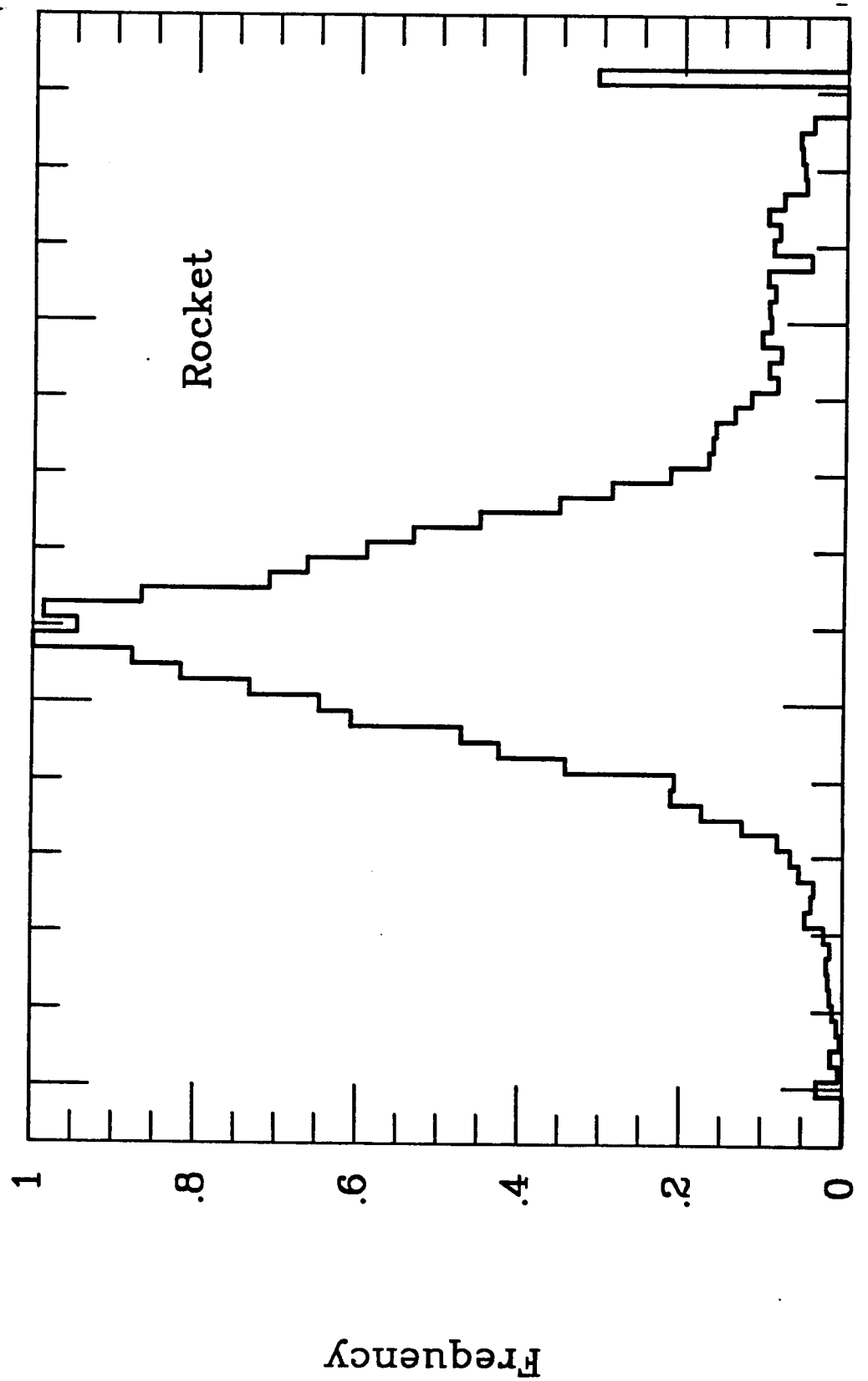

Figure 16. Distribution of total charge amplitudes for events recorded by the CCD on the rocket flight. We have yet to explain the events with anomalously large amplitudes ($\gtrsim 200$). The tall bar on the right hand side represents all events with signal amplitudes ≥ 255.

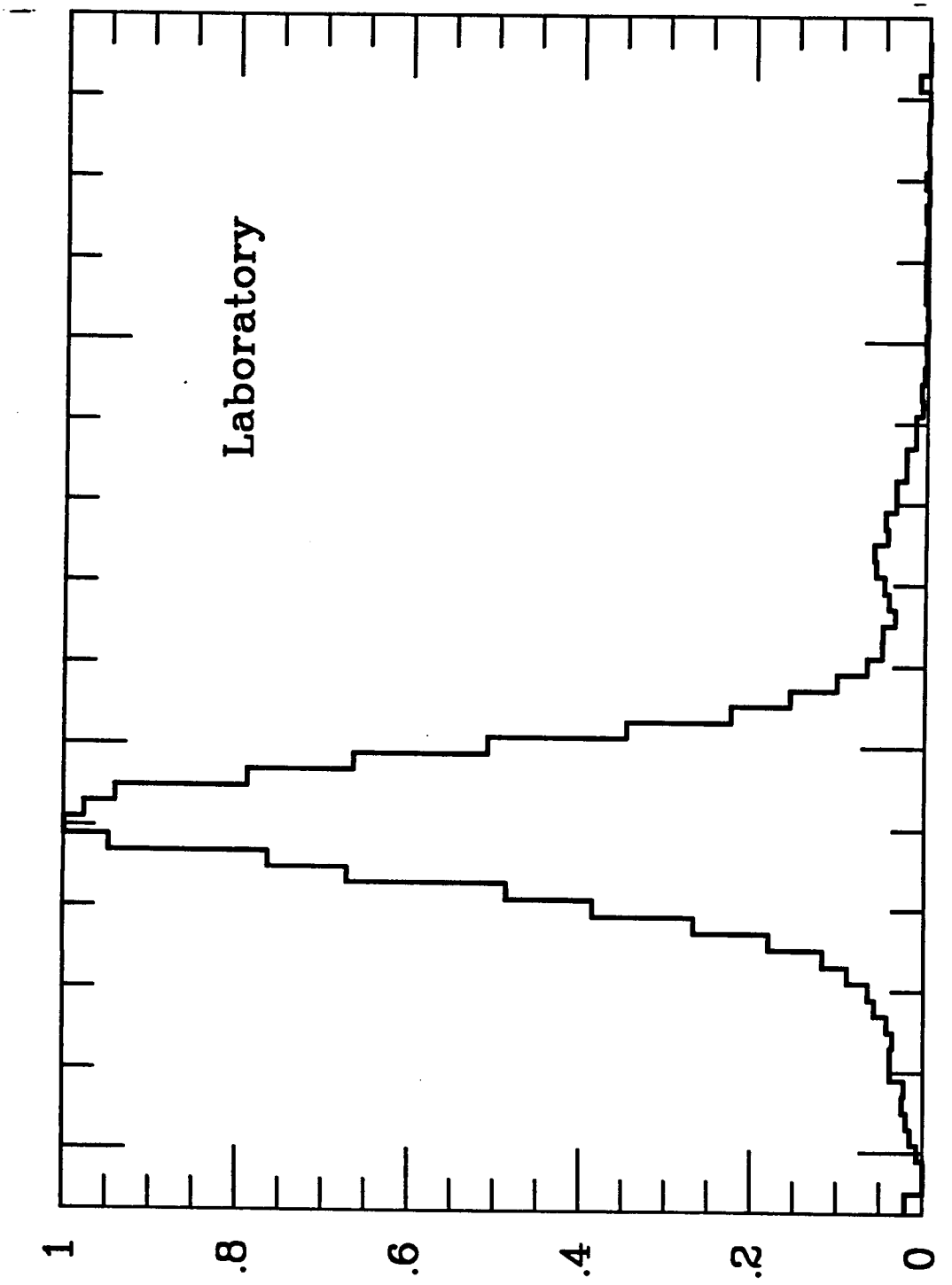

Figure 17. Same as for Fig. 16, except that the results are from the CCD tested in the laboratory. Note that the anomalous peak on the right is not at a signal level twice that of the main peak's center. Hence, it is unlikely that the second peak represents detections of pairs of nearly coincident events.

Consider the histograms shown in Figures 16 and 17 which illustrate that the rms dispersion of signal amplitudes σ_Q equals 0.22 times the modal amplitude Q_m. An important issue is how important the charge fluctuations should be in practice. Since the random processes which influence (1) the counting statistics, (2) the signal amplitude once an event is present, and (3) the readout noise level are all statistically independent processes, the net signal variance is the sum of the variances arising from the three processes. If we normalize these variances to that of the Poisson counting fluctuations, we find the deterioration factor F for the SNR (i.e., how much worse the SNR will be, compared with perfect counting) is given by the relation

$$F = \left[1 + \frac{\sigma_Q^2}{Q_m^2} + \frac{\sigma_r^2}{R Q_m^2} \right]^{1/2}$$

where R is the average rate of events per pixel in each frame, for a specified level of intensity, and σ_r is the readout noise per pixel in a single frame. If we omit the third term in the equation we find for $\sigma_Q / Q_m = 0.22$ that R is only 1.024.

In the context of analog integration, it is instructive to grasp an approximate value for the dynamic range of the ICCD. Suppose we define the bottom end of this range to be where the SNR is decreased by a factor $F = \sqrt{2}$ from pure photon counting fluctuations. For $Q_m / \sigma_r = 25$, this condition is satisfied when the intensity level $R = 0.0016$ events pix^{-1} frame^{-1}. We may consider the top end of the dynamic range as that where, in a single frame, the full well capacity is reached in the CCD pixels. For the sake of argument, if a particular CCD has a capacity of 2×10^5 e^-, we can have $R = 70$. To summarize, we find that the dynamic range $R_{top} / R_{bottom} = 40{,}000$, regardless of how rapid the frame rate is.

The dynamic range for photon counting is bounded at the top end by the need to avoid overlap of nearly coincident photoelectron hits which might be confused as a single event (say, $R < 1/9$ or so). The bottom end of the range is virtually limited by only one's patience to achieve a reasonable SNR in the end, or perhaps by dark count, ion events, etc.

6. Development of a Flight ICCD Unit

6.1. Background

In 1978 NASA released an announcement of opportunity (AO) which requested research groups to submit proposals for experiments to be flown on future Spacelab missions. In response to that AO, Princeton University and the Ball Aerospace Systems Division (BASD at Boulder, Colorado) teamed up to submit a proposal in November of that year to fly a high-resolution spectrograph for observing hot stars in the ultraviolet. The payload instrument, called the Interstellar Medium Absorption Profile Spectrograph (IMAPS), was an ultraviolet echelle spectrograph which could record stellar spectra from 965 to 1165Åwith a wavelength resolving power $\lambda/\Delta\lambda = 2\times10^5$ (i.e., < 0.01Å).

There was a two-fold motivation for building and flying IMAPS, one scientific and the other technical. The scientific purpose was to establish an observing program with an instrument which could reach beyond the capabilities of the telescope-spectrometer built by Princeton for the *Copernicus* satellite. This new initiative was to build upon the earlier pioneering conclusions on the nature of the diffuse interstellar medium which were derived from the many years of operation of *Copernicus*. Specifically, we felt a strong need for having an instrument which could record stellar spectra in the astrophysically important wavelength range extending from the Lyman limit (912Å) to the vicinity of 1100 to 1200Å, but with significantly higher wavelength resolving power than that provided by *Copernicus* ($\lambda/\Delta\lambda = 20{,}000$).

The main technical objective was to have a program which made use of the windowless, oblique-focus ICCD detector developed under this grant. We felt that beyond the immediate need to achieve the goals of the IMAPS scientific program, this detector represented a very promising candidate concept for a two-dimensional image sensor to be used on future space astronomy enterprises which must function at wavelengths covered by IMAPS (such as the proposed *Lyman [FUSE]* Explorer mission). True enough, there are other detector configurations suitable for far-uv wavelengths which use a microchannel plate with a

photocathode deposited on the front surface. However, photocathodes operating on the rugged terrain of an MCP have two drawbacks, of as yet undetermined severity, when compared with monolithic photocathodes on a solid substrate employed by the Princeton ICCD. The discontinuous structure and complicated $\vec{E}$ fields of the MCP photocathodes result in 1) a lower overall quantum efficiency and 2) spatially periodic modulations in response caused by the MCP pore structures which can produce undesirable effects if the images have small-scale details. The latter effect has yet to be measured directly, but its existence seems very plausible. By 1978, our concept for the ICCD was well enough developed to justify our undertaking a flight instrument development as a logical means to bring forth a more mature design. Also, we knew that ultimately we would need to prove that the detector could function well in an actual flight environment before it would be an acceptable candidate for ultraviolet instrumentation in general.

On the basis of a Category III rating by the peer review of our proposal, NASA turned down our request for a Spacelab mission assignment. While the proposal was judged to have excellent scientific merit, some apprehension was expressed about the technical risk in trying to fly a detector which was not proven. On the basis of this evaluation, we felt it was proper to resubmit our proposal within the framework of a sounding rocket research program. The appropriateness of this strategy was underscored by the basic philosophy of the NASA sounding rocket research effort, namely, to allow investigators to develop new instrument concepts at low cost, with a generous flexibility in schedule, and without the risk that technical difficulties or initial flight failures would jeopardize the large investment of a complex flight program.

The initial submission of a proposal for sounding rocket research using the IMAPS instrument was made in July 1979. This proposal was followed by amended budgets and schedules in November 1979 and March 1980. On August 21,1980, NASA awarded (through the Goddard Space Flight Center) contract NAS5-26268 to Princeton University to embark upon the proposed program. Thus, for the most part, the research and development efforts of the NASA grant NSG-7618 were performed concurrently with the more specific design and fabrication

work for a flight unit which was supported by the sounding-rocket program.

6.2. Historical Summary of the IMAPS Sounding Rocket Program

The design, procurement of parts and assembly operations at BASD advanced in an orderly fashion from late 1980 to mid-1982. The image section of the detector was designed at BASD, while Princeton had responsibility for supplying the CCD and its associated clocking and video detection electronics. To a good approximation, we were able to maintain the program within the projected costs and schedule throughout these phases. After the basic payload fabrication had been completed in late 1982, NASA support was shifted from the contract to a grant (NAG5-616) since the remaining effort was to be primarily mission operations, payload refurbishment and scientific research, rather than the initial procurement of a complicated instrument from a subcontractor.

In preparing the payload for flight, we experienced a delay of about one year after we discovered the sensitivity of IMAPS was at least one or two orders of magnitude too low. Ultimately, we traced the difficulty to problems with the detector. Specifically, the design of the on-chip amplifier for the CCD that we purchased initially was not good enough to give us the necessary charge sensitivity and high-frequency response to detect individual photoelectrons. Also, its charge transfer efficiency was not adequate. In early 1984 we obtained from RCA a CCD with a newer design. This CCD showed excellent operating characteristics, and as a result, the earlier difficulties with our detector were surmounted very effectively.

The first launch of the IMAPS instrument on a Black Brant rocket occurred on October 5, 1984. Unfortunately, on this flight there was a catastrophic inrush of air into the payload. The severely degraded vacuum caused the detector's high voltage system to break down and as a result we were unable to obtain any data. An analysis of the probable cause of this failure is discussed in detail in the final report for the initial contract and will not be repeated here.

Shortly after the first flight of IMAPS, BASD began refurbishment of the payload for a second flight. Concurrently, we started an investigation on what caused the vacuum failure

and what steps we would take to minimize the chances that it could occur again. After we had satisfied ourselves that we had worked on the vacuum problem as thoroughly as possible, we embarked on final preparations for the second flight.

The second flight of IMAPS occurred on April 20, 1985. All of the payload systems functioned perfectly, and excellent recordings of the data were obtained. We were not only pleased with the quality and quantity of scientific information available from this flight, but also we gathered valuable indications on how well the ICCD image sensor can perform in a space environment. A discussion of these conclusions from the flight data are contained in §§ **4.2**, **5**, and **6.3**.

In response to a solicitation from NASA Headquarters to existing sounding rocket experimenters, we submitted a proposal in June 1984 to convert IMAPS for operation on Spartan and fly it in early 1988. In early 1985 we learned that NASA accepted our proposal, and we embarked on a program to reconfigure the payload so that it would operate on Spartan. Following the disaster with the Challenger Space Shuttle and the strong indication of a very bleak outlook for future manifesting of Spartans, we redirected our energy to preparing IMAPS for more sounding rocket flights.

6.3. IMAPS Instrument Overview

The IMAPS payload was a slitless, objective grating spectrograph which recorded ultraviolet stellar spectra at a resolution of approximately 0.004Å (profile FWHM) and with a sample interval (pixel width) of 0.002Å over the very difficult wavelength range $965 < \lambda < 1165$Å. A key feature of the optical design was its extreme simplicity; aside from a mechanical collimator which restricts the field of view to a one degree circle to eliminate confusion from nearby stars, the incident starlight interacts with only two optical elements before it is imaged. First, the parallel beam hits an echelle grating. Diffracted light from the echelle then goes to a parabolic cross-disperser grating which images the spectrum on a 1.5 cm diameter photocathode in a windowless, photon-counting Intensified CCD detector (ICCD). The system is illustrated in

Figure 18.

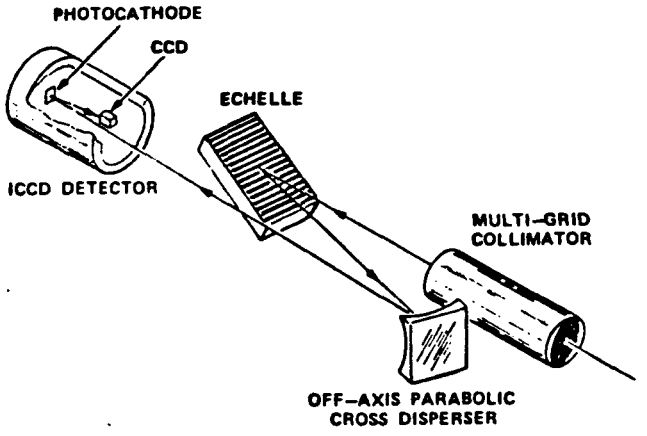

Figure 18. Optical layout of the IMAPS sounding rocket payload.

The high wavelength dispersion of this instrument was achieved by having the echelle set at a large angle of incidence (63°) and employing a very long focal length for the cross-disperser (1800 mm). While the area of the entrance aperture was only 250 cm^2, the light collecting power of the instrument was very good for a device working in this wavelength interval because there were relatively few reflections and the KBr photocathode, being opaque and on a solid substrate, had a high quantum efficiency. This payload was built to fit within the standard Black Brant sounding rocket envelope (17-inch diameter cylinder).

6.4. Detector Design

As emphasized earlier (§1), short-wavelength photons must be allowed to reach the photosensitive medium without having to penetrate any sort of window, since bulk pieces of even the best optical substance (LiF) are virtually opaque to such radiation. Indeed, it is for just this reason that such general-purpose, uv observing facilities as *IUE* and the (first generation) spectrographs aboard the *Hubble Space Telescope* are unable to operate over nearly all of the very profitable wavelength range covered by IMAPS.

The IMAPS spectrograph casts its image onto a photocathode which consists of a layer of KBr on a solid substrate exposed to the vacuum environment. The quantum efficiency of an opaque photocathode of this type, approximately 77% near the middle of our spectral cover-

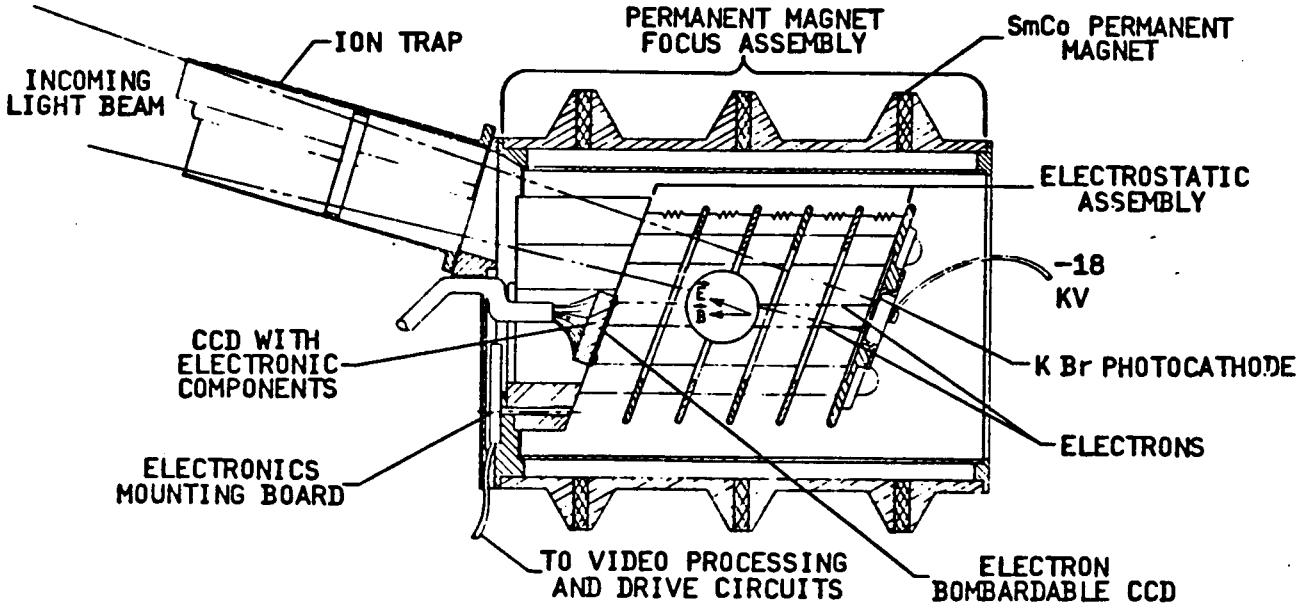

Figure 19. Image section of the windowless, oblique-focus ICCD detector constructed for IMAPS.

Inside the IMAPS ICCD image section, electrons emitted off the front face of the photocathode are accelerated by a 19 kV potential toward an RCA (SID-501) CCD with 320×256 separate charge collecting wells, each with a square dimension of 30μ. As illustrated in Figure 19, a magnetic focusing field is inclined to the voltage gradient by a small angle (20°) to allow the electrons to diverge from the optical beam and hit the CCD. From laboratory tests using a patterned photocathode (shadow evaporated through a standard Air Force bar-chart test pattern), we were able to verify that the oblique focus arrangement for the electrons produces as sharp an image as the CCD is able to show us. Theoretical calculations of the focusing properties of the oblique configuration gave a 6μ diameter for the electron spot emitted by a single point on the photocathode.

So that it can respond to direct electron bombardment, the CCD has its normal supporting layer of cover glass etched away. The entire field of the CCD is read out 15 times a second. It is not necessary to cool the CCD, because not very much dark current is accumulated over the 1/15 second duration of an exposure. (A more rapid frame rate would have been desirable, since we could have tolerated a higher count rate per pixel for bright sources without coincidence losses, and there would be less image smear when the rocket pointing moved -- see §**6.6**. However, several limitations prevented this higher rate: (1) Clocking pulse rise and fall times were not sharp enough -- see the discussion near the end of §**6.7**, (2) We did not have sufficient telemetry bandwidth to handle the faster pixel readout rate, and (3) We needed to keep the number of frames which had to be digitized and analyzed to a reasonable number.)

If ions enter the ICCD image section, or are created therein, they are accelerated toward the photocathode. When they hit, they each produce a bunch of electrons (about 10 or 20 in number) which will, in turn, register as a great big event on the CCD. As long as these ions events are not so numerous that the detector field becomes much too busy, we can make them have virtually no influence on our observations because they are easily recognized (because of their large amplitude) and can be rejected by the event-detection processing by a computer after flight. In our laboratory vacuum tests of the IMAPS ICCD, we found that the ion event rate was very low (only a few events per 1/15 second frame), and there was very little increase when we deliberately let the pressure degrade to 2×10^{-4}torr. Likewise, on the successful sounding rocket flight, the ion rate was very low (see §**6.6.3**).

The low ion rate we experience with the detector is probably attributable to a number of precautions that we have built into the design. First, the optical system and the detector are enclosed in a cylindrical vacuum vessel which is always pumped down for a long period of time before flight. This pumpdown virtually eliminates outgassing from adsorbed volatiles or trapped gases (within small voids) inside the payload. As a second precaution, we installed an ion trap in front of the detector and put the mechanical collimator (the only opening to the outside) at a slightly positive potential with respect to the outer shell of the payload. Finally,

we have found from our laboratory testing that the most important parameter for keeping the ion rate low is cleanliness of the payload components, especially those associated with the image section. In recognition of this, we thoroughly cleaned and vacuum baked the ICCD assembly.

6.5. Signal Transmission

For sounding-rocket flights, we amplified the raw video signal from the CCD, packaged the information into the standard broadcast TV signal and synchronization protocol (but with each CCD row expressed in 4 TV lines, resulting in 2 TV frames per CCD frame), and then the signal was transmitted on a broad-band telemetry channel to ground for recording on a VCR tape. After flight, the analog video recordings were digitized, and the photoevents were subsequently recognized and centroided by computer processing.

6.6. Compensation for Small Pointing Errors

There is no active system to stabilize the wandering of a spectrum while the rocket's attitude moves within the ACS limit cycle. Instead, a small mirror[1] ($\sim$1 cm^2 in area) attached to the echelle grating directs a broad-band image of the target star to the cross disperser which in turn focuses it near one edge of the ICCD picture format. As the spectrum moves in x or y, this bright, point image moves in precisely the same manner, and we use it as a position reference in each recorded frame. As long as the rate of angular motion is less than about 5" s^{-1}, the smearing of spectral detail in a single 1/15 second frame will be completely negligible (a 15μ sample is equivalent to 1.72" in the sky). Even the worst angular rate quoted for the Strap 5 ACS (10" jitter peak to peak @ 0.2 Hz $\equiv$ 4" s^{-1}) should be within this tolerance (but it wasn't on the mission flown in 1985).

[1]There are actually 5 such mirrors installed on the echelle housing, one for each of the 4 tip positions and an extra one on an opposite side of the echelle to serve as a focus monitor in one of the positions.

6.7. Interim Problems with CCD Performance

In preparation for its first flight, in February 1983 the IMAPS payload underwent the standard integration and evaluations at GSFC (e.g., tracker alignment, electrical functional tests, determination and adjustment of the center of mass, bend tests, spin balancing vibration tests and post-T&E integration). In addition, we evaluated signal transmission quality of our ICCD output throughout the telemetry system. Overall, the outcome of the GSFC integration tests were uneventful, and the payload was successfully integrated with the rest of the rocket systems.

After the integration run at GSFC, we transported the payload to the Naval Research Laboratory (NRL), where G. Carruthers had a test facility which permitted us to evaluate the performance of the complete payload assembly for imagery of spectra. After about five days of intensive testing and problem solving, we ascertained that the payload had an enormous loss of sensitivity. We could detect a signal only when the test apparatus was emitting a flux far above what we could ever expect from a celestial source. At the time, we were unable to determine whether the problem was relatively trivial, such as from a simple mechanical interference in the beam or a grating being off its blaze, or more fundamental, such as an insensitive detector or nonfunctioning optical component. Since it was clear that we could not fly the instrument under the circumstances, we postponed the flight and shipped the payload back to BASD for trouble shooting.

Our initial suspicion was that there was no fault with the CCD, because we thought we were able to register the presence of individual photoelectrons and our problem was simply that there were few in number (that conclusion, as later investigations revealed, was definitely false!). Thus, in the early phases of trouble shooting, we concentrated on possible sensitivity losses in the optical system.

Extensive testing of different optical components, together with independent confirmations that they were installed correctly, failed to reveal identifiable problems. Thus, our attention turned to locating possible deficiencies of the detector. From previous tests of

electron yields from single photoevents, measurements of the CCD on-chip amplifier gains, and our experience with the random noise at the output, we would have predicted that single photoevents would have had a healthy 20:1 signal-to-noise ratio. On the other hand, examination of the recorded data showed that the photoevents were not too easily recognized, and in addition, they seemed to show a large dispersion in amplitudes. In one diagnostic session with the camera electronics, we discovered an open circuit in the CCD amplifier reset line, caused by a wire which had come loose from a connector. After correcting this problem we found an improvement in the recognizability of events, but the overall sensitivity of the detector had not improved. G. Carruthers remeasured the quantum efficiency of the photocathode at NRL. While some loss of efficiency had occurred, it was only by a factor of three at the very most -- far short of the amount needed to explain our sensitivity problem.

The complete ICCD detector and associated electronics were shipped to Princeton for further study. In support of the research discussed in §7, we had on hand a uv source whose absolute flux had been calibrated. It consisted of a radioactive source which produced Cerenkov light in a MgF_2 crystal at the focus of a collimating mirror. The yield from the source should have produced 400 events per second over the complete ICCD frame area, yet we were unable to see any events whatsoever, when we viewed the video output on a monitor screen. Ultimately, this test convinced us that our fundamental problem rested with the apparent inability of the CCD to show us *single* photoevents. In the past, we thought we could see such events when the detector was exposed to bright uv sources. However, these sources were so bright that what we were indeed seeing (and interpreting as single events) were the chance pile-ups of multiple electron hits on top of a crowded sea of photoevents.

This conclusion was surprising at the time, since, at least superficially, straightforward calculations of the overall sensitivity seemed to indicate that we would have had no difficulty in registering single events. Specifically, we knew that from previous experiments with the CCD operated in slow-scan mode (long integration times, CCD cooled to -130 °C, 10 second readout time for a whole frame) that the charge yield for 17 keV electrons was about 4000

electrons per event. The charge sensitivity for the on-chip amplifier at the high bandwidths needed to record at the IMAPS fast scan rates was $0.25\mu V/e^-$ when it was connected to a $3K\Omega$ load of the IMAPS video amplifier. While this gain was lower than the nominal value of about 0.5 to $1.5\mu V/e^-$ found for this and similar RCA CCDs, by itself this reduction could not explain why we were unable to see events. An additional effect, however, conspired to reduce our signal margins farther. From experiments at slow-scan rates with several different CCDs viewing an optical test pattern, we knew that pulses only one pixel wide experienced a loss of signal amplitude by about a factor of two, compared to illuminations which covered a large number of contiguous pixels. Even so, we calculated that 17 keV charge packets passing through the IMAPS signal chain with its gain of 560 would produce pulses with an amplitude of 280 mV, if all of the charge were concentrated in a single pixel. Compared with measured rms noise levels ranging from 24 to 36 mV, we expected a signal-to-noise ratio (total charge to readout noise in a single pixel) somewhere between 8 and 12. While this was ostensibly a reasonable margin for detection, we nevertheless harbored an awareness that, at the higher clocking rates needed for IMAPS, any further reductions in the CCD's charge transfer efficiency (CTE) could compound the attenuation of point-like signals and jeopardize our ability to perceive the events.

Following these initial conclusions, we embarked on an intensive evaluation of many different CCDs. Our goal was first to obtain a better perspective on the limitations of then currently available devices and then explore what corrective actions we could take to restore the IMAPS ICCD to a condition where we could unquestionably record individual events. As a first step, we tested two CCDs purchased for another NASA grant program at Princeton (for an optical observing camera for ground-based telescopes). These CCDs, virtually identical to the RCA type 501 scientific chips selected for the IMAPS detector, were assemblies mounted on glass (hence they were not electron bombardable).

While both devices showed good responsiveness in their on-chip, dual stage output amplifiers, 1.5 $\mu V/e^-$ for one device and 1.4 $\mu V/e^-$ for the other (which was a major

improvement over the earlier 501 chip designs), they still had rather poor parallel CTE, even after we had experimented with changes in the rise and fall times of the vertical (parallel) clocking waveforms. For both chips the CTE was bad even at high signal levels or during operation at -80 ° C (often, CCDs show poor CTE only at low signal levels and low operating temperatures; the problem usually clears up for strong signals). Specifically, the poor CTE degraded a spot illumination of a single pixel with a level of 12,000 e^-/pixel to a point that it couldn't be seen above the noise on a repetitive oscilloscope tracing of a single line's readout. This pixel was located near the center of the field. Another pixel near the top of the A register which was illuminated with the same single-pixel spot couldn't be seen until the signal went above 21,000 e^-/pixel! The appearance of a bar-chart test pattern indicated that the serial CTE for these devices was good however. We also noted that the readout noise levels were a bit on the high side: one device showed a noise of 200 e^- rms in the active pixels and 160 e^- rms in the overscan area, while the other showed respective values of 150 and 130 e^- rms. These CCDs were eventually returned to RCA because we felt that they were unsatisfactory.

After the above mentioned tests were completed, it became clear that major improvements in CCD performance were needed to achieve our objective of registering individual electron events at the IMAPS frame rates. In the summer of 1983, we were informed by RCA that a new design of CCD would be produced which, they claimed, would have somewhat better performance. We responded by placing an order for this new device, with a specific request that it have the cover glass chemically etched away so that the CCD would be electron bombardable. At the time, we were informed that the new CCD would be shipped several weeks after we placed the order. As things turned out, however, it didn't arrive in Princeton until early December of that year. This delay in the procurement created a significant slip in the IMAPS program schedule.

As with the two CCDs used for ground-based observing, the amplifier exhibited good gain ($1.3\mu V/e^-$) but with this device the serial CTE was not especially good. In contrast to the earlier two chips, however, we found that the CTE was acceptable with moderately large signal

pulses, or with small signals on top of an elevated zero-level background (around 25 mV). In fact, with a signal bias from the high dark current that we could anticipate for normal fast scan operation at room temperature for the IMAPS camera, we ascertained the CTE would be acceptable, that is, individual photon events would not become unrecognizable. The noise level in slow scan operation was equivalent to 110 e^- rms, which for IMAPS operations was a good figure. One disturbing feature of this particular CCD was that its quantum efficiency showed strong variations over the field. A flat field exposure showed global fluctuations of about 50% in amplitude. While this probably would not present a serious operational problem for IMAPS, the lack of uniformity indicated that there might have been some problems with quality control in the manufacturing process.

Shortly after the evaluations of the first new IMAPS CCD had begun, we had the opportunity to check out a much newer CCD purchased by the image sensor development group at Princeton's Plasma Physics Laboratory (PPL). This CCD was from a brand-new batch produced at RCA. We learned from RCA that this newest batch had some processing improvements incorporated into their manufacturing procedures. It was immediately apparent to us that the PPL chip was significantly better than any chip we had seen before. The CTE for this chip was excellent all the way down to signals of 1000 e^-/pixel (single pixels could be seen at that level). A surprisingly high gain of 2.6 $\mu V/e^-$ was found at the output of the amplifier, and the noise was only 60 e^- rms. The response to a flat field illumination was quite uniform, and there were no blemishes, hot pixels or bad columns. Another very extraordinary feature of this chip was that the dark current was quite low. In the slow scan test set, which normally clocks out the CCDs at a rate which gives an effective integration time of 10 seconds per frame, the dark current at room temperature gave a charge equal to only 3/4 of the full well capacity of the pixels!

On the basis of the very favorable results we obtained for the PPL CCD, we decided to place immediately a new CCD order for the IMAPS program. We were especially anxious to obtain a device from the same production run as that which generated the device which

belonged to PPL. Also, we felt that it was important to have a backup chip to support our flight operations.

The second IMAPS chip arrived in Princeton in mid January of 1984. Much to our delight, we found that the slow-scan performance of this chip seemed to be about as good as the PPL one. The noise was only about 90 e^- rms, and once again the thermal dark current seemed extraordinarily low at room temperatures. Both the serial and parallel CTE at slow scan seemed to be excellent. We had no trouble seeing a single pixel illuminated at a level of 2000 e^-/pixel, which is a weaker spot than we'd expect from single 15 to 20 keV electrons in the IMAPS ICCD. The sensitivity of the output amplifier was again as good as we had seen in recent CCDs from RCA: 1.4 $\mu V/e^-$. Also, a very clean format with a uniform flat field response was observed.

When we installed the new CCD in the IMAPS breadboard fast scan camera system, we were were pleased to see that the charge sensitivity of the output stage was, as close as we could determine, as good as the slow-scan performance. This was an important improvement over the CCDs which we had purchased much earlier for the IMAPS program. However, the fast-scan testing also gave us a preview to some unanticipated technical hurdles. It was immediately apparent that the very fine CTE we could obtain at slow scan rates was no longer in evidence in the fast scan camera: in essence, things had really gone to pot! (We never experienced a loss of CTE going from slow scan to fast scan in our evaluations of CCDs in past years.)

After some investigation, we determined that the source of this new CTE problem was indirectly a result of the new construction of the CCDs. To overcome the more fundamental lack of good CTE in their devices, RCA modified the construction of the gates from an open strip configuration to a more highly overlapping sandwich-type layout. This type of construction was intended to reduce the losses resulting from field fringing at the gate boundaries when the phases were switched, and the excellent CTE we were finding at slow scan rates confirmed that the new design strategy was working well. However, a byproduct of the new construction

was that the interelectrode capacitances were significantly higher than in the old design. As a consequence, with our current electronics we were unable to impose properly shaped waveforms on the input pins of the clocking gates. Based on advice we received from RCA Laboratories, we concluded that the high capacitance resulted in a bad impedance mismatch through the 3 or 4 inch leads between the clocking output drivers and the CCD. They advised us that leads longer than an inch or so were bound to give us difficulties in obtaining the necessarily sharp waveforms to do really fast transfers. Also, the output driver stages in our camera didn't seem to have enough current capacity to do the job. We experimented with shorter lead lengths and extra emitter follower stages to help us obtain better waveforms at the CCD and hence improve the CTE, but only a mild improvement was seen.

While we could have gone to more extreme measures to improve the clocking drives and physically relocate the circuits, such changes would have forced us to do a major rebuilding of the flight camera. The modifications would have entailed our putting the output driver stages very near the image section -- an undesirable option in view of the probable outgassing from the circuit elements which are dissipating a large amount of heat. Even then, we judged that there might still be some risk that we would be operating the chip clocking under marginal circumstances. In the light of this, and again following the advice from RCA, we decided that the best course of action was to relax on the whole timing scale and reduce the overall frame rate of the IMAPS camera by a factor of two. Thus, we would operate the camera at 15 frames per second instead of an originally planned rate of 30. Indeed, when we experimentally reduced the master clock frequency by this factor of two in the breadboard camera, we were able to clock the CCD much more comfortably, and the good CTE returned.

In summary, we felt that our position *vis-a-vis* CCD performance had improved markedly over our situation of approximately a year earlier, when we discovered that the IMAPS instrument sensitivity was falling far short of our expectations. The new RCA chip design had a number of important improvements which reflected very favorably on our ability to detect single high-energy photoelectrons in the IMAPS image section:

[1] The single level gate electrodes were replaced by multilayer, overlapping gate structures to improve the CTE.

[2] The single video output transistor on the chip has been replaced by two amplifiers working in cascade. This resulted in a more predictable output response (from one device to the next) and seeed to prevent the signal loss which occurs when the sample times are shortened (at fast scan) or when the output impedance is lowered (the input impedance of the IMAPS camera circuits was only $3K\Omega$). At fast frame rates the improvement in charge sensitivity seemed to be about a factor of 3 over the earlier devices. Also, the readout noise, expressed in terms of equivalent electrons per pixel, was about a factor of two lower in fast scan applications.

[3] Better manufacturing procedures or higher quality silicon in the new CCDs evidently gave us devices with very much lower thermal dark currents and formats which have very few cosmetic problems. The flat-field response also seemed to be excellent. While these considerations were not too vital for IMAPS applications (aside from making the data reduction a bit easier), they indicated that the overall quality of the product had improved, which probably also reflected favorably on its survivability.

[4] Some of the signal lines leading to and from the on-chip amplifier had better shielding from the clocking leads. As a consequence, the instantaneous levels detected by the IMAPS sample-and-hold modules were less subject to interference from the tails of the clocking pulses. We later realized that this change gave us a vastly lower response to interference from noise pulses from the voltage regulators in the electronics power supply. Evidently, the carry-over of the pulses into the video signal was caused by part of the video sampling riding up on the steep exponential tails of the previously enormous clock pulses in the CCD's raw output.

[5] The new CCDs had a much better pin design. We could expect to see a significant improvement in the reliability of the electrical connections to the device, especially under the severe environmental conditions of a rocket flight.

6.8. Conclusions from the Flight of IMAPS on a Sounding Rocket (27.082UG)

The IMAPS mission flown on April 20, 1985 (0050 MST) was a complete success, both technically and scientifically. The target on this mission was π Scorpii, a B1V+B2V type star (actually a binary system with one component very much fainter than the other) with a V magnitude of 2.88. From the real-time TV display of the detector output telemetry signal, it was immediately apparent that the payload was stabilized on target, that the detector was functioning very well, and that a spectrum of about the right intensity was being registered. It was also clear that the Lyman-α airglow background was at about the expected level -- i.e., not strong enough to compromise the data quality.

Many of the conclusions on the properties of photoevents recorded on this flight (charge amplitudes and spreading properties) have been presented earlier in this report (§§ **4.2** and **5**). We summarize below a few other observations about the detector performance on the flight.

6.8.1. Signal-to-Noise Ratio (Conspicuousness of Events)

In Figure 16 (§**6**), if one rejects the extended tail of the distribution at the high end by substituting in the dropoff at the low end, reflected about the distribution's axis of symmetry, one finds that the average pulse amplitude is 118.5 and the *rms* dispersion is 26.1. The peak is well separated from the random noise in the readout, which, on the scale given in the figure, corresponds to an *rms* variation of 4.81.[2]

[2]The noise in the digitized versions of the flight frames is greater than measured variations in the analog telemetry signal. (For instance, digitized SNR = 118.5/4.81 = 24.6, while the pulses seen on the raw VCR output -- ranging from approximately 200 - 250 mV -- have a *minimum* SNR = 200/5.5 = 36.) The source of this extra noise is not understood at the moment. It may be attributable to either problems with our Colorado Video digitizer or with the VCR when it operates in the freeze frame mode.

6.8.2. General Appearance of a Frame

Figure 20 shows a single frame recorded on the flight. A blowup of a panel near the bottom (Fig. 21) clearly shows photoevents as large spikes, spread over one, sometimes two, and very occasionally three or four CCD wells (depending on whether or not the incident photoelectron landed near a well boundary). The echelle orders are barely perceptible as linear groupings of events stretching horizontally. At the bottom of the picture is the very bright image of the star formed by one of the mirrors described in §**6.6**. The top half of the format is very busy with events and had to be analyzed by analog coadding of pixel amplitudes. Away from the bright portion of the picture event recognition could be accomplished.

The picture is divided into 16 panels because there were interruptions which occurred during the standard TV broadcast line and vertical retrace intervals (see §**6.5**). The thin, rectangular blocks of pixels which appear to be anomalous in the upper right portions of each panel do not contain valid image information; these pixels were overwritten by the character insertion generator which was used to identify the precise time each frame was recorded (the character information is scrambled when the broadcast TV image's interlaced lines are rearranged for the IMAPS detector display -- portions of the unscrambled numbers are written on the right hand edge of the picture).

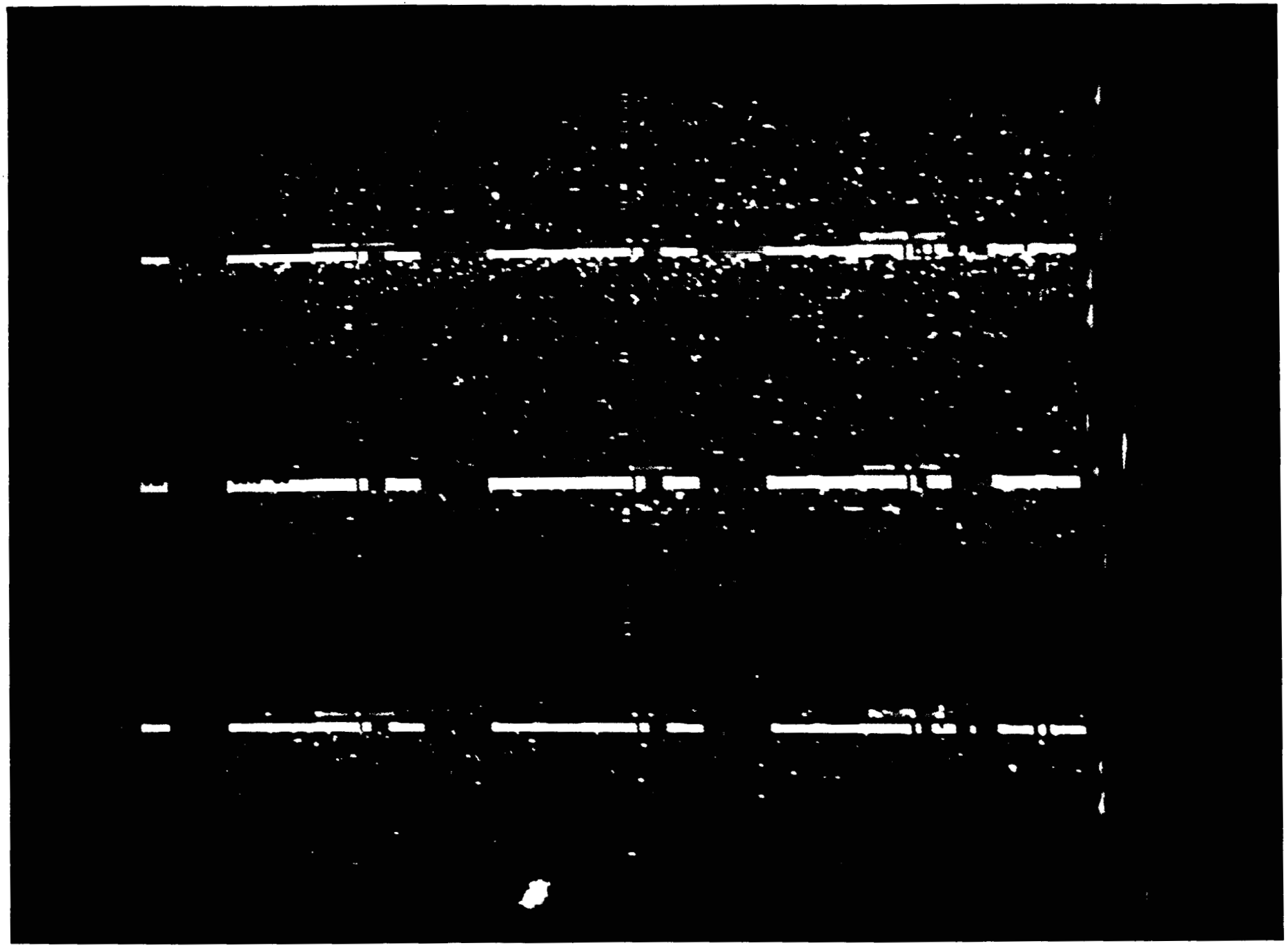

Figure 20. One of 4,300 frames of ICCD data obtained from the sounding rocket flight which recorded the far-uv spectrum of the early-type star π Sco. Each bright speck represents a single photoevent which impacted the CCD in the 1/15 second frame time. The bright spot at the bottom is the broad-band image of the star which indicates the instantaneous offset of the spectrum caused by angular motions of the payload.

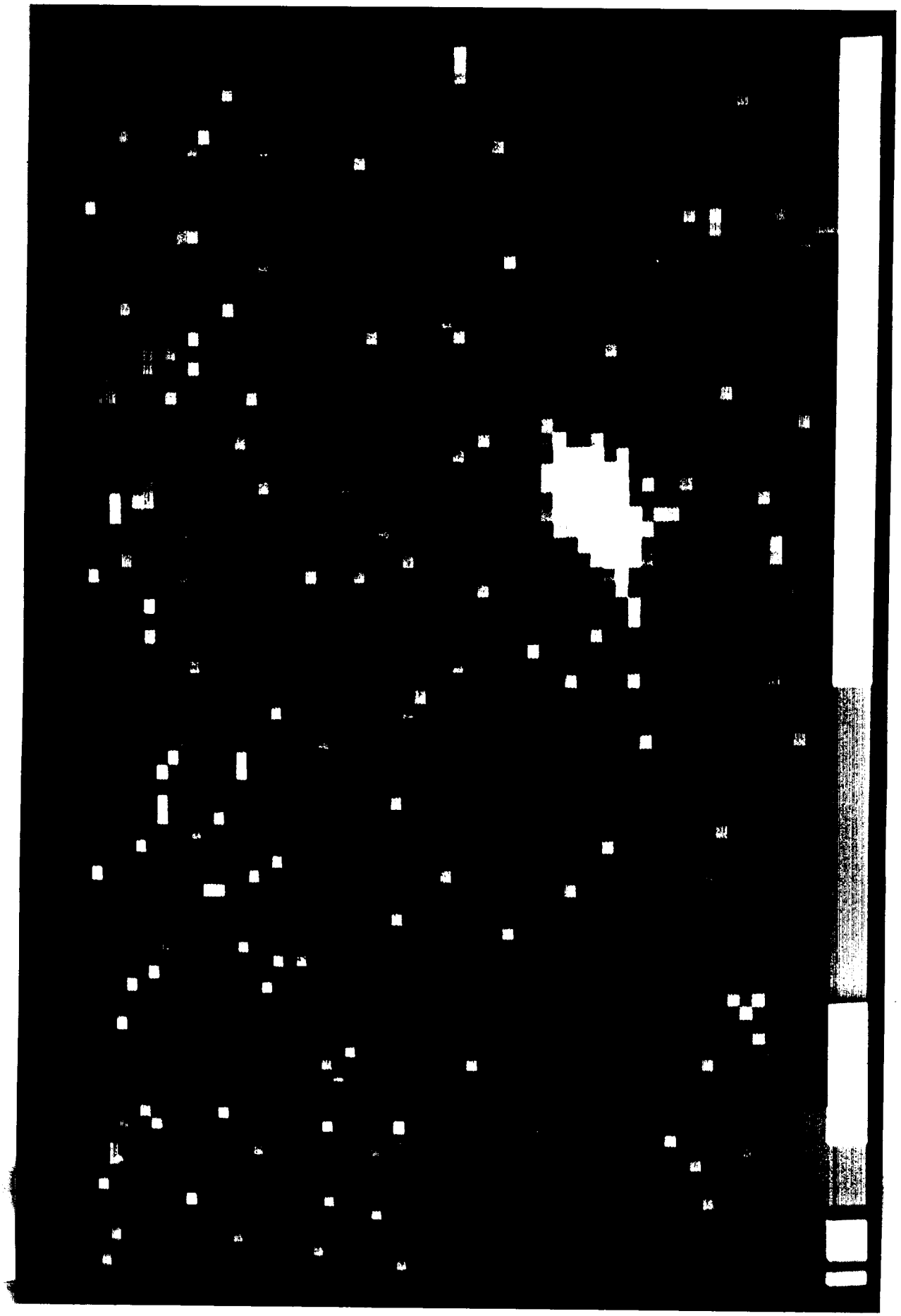

Figure 21. An enlargement of one of the bottom panels in Figure 20, showing the detail of intensities in individual CCD pixels.

6.8.3. Rate of Ion Events

For 70 frames which were recorded at an altitude of 270 km (very near apogee), there appeared to be a total of 73 ion events. The actual number of events may be lower than this number because some of the spikes with large amplitudes may have been multiple (legitimate) photoelectrons. The 73 hits in 70 frames translates to an event rate of 1.9×10^{-4} hits pix^{-1} s^{-1}.

6.8.4. Sensitivity of the Entire Instrument

A measurement of the continuum of π Sco between 1141.00 and 1141.20Å gave an average count rate of 0.75 count pix^{-1} frame^{-1}. This level refers to the intensity above a background composed of scattered light plus the diffuse Lα background. We estimated the true flux from π Sco within this wavelength interval by two methods: 1) The low-resolution (U2) *Copernicus* scans of this star reported by Snow and Jenkins[3], using an average of the counts recorded at the two end-point wavelengths and their reported sensitivity of the *Copernicus* spectrometer at the time, and 2) *IUE* absolute fluxes near 1140Å for the V = 6.15 magnitude B1V star HD31726.[4]. The IUE intensity of 7.5×10^{-10} erg cm^{-2} s^{-1} Å^{-1} (= 42.8 phot cm^{-2} s^{-1} Å^{-1}) was multiplied by a factor of $10^{0.4(6.15 - 2.90)}$ to account for the differences in visual magnitudes and $10^{-0.4(0.03)(8.1)}$ to correct for the fact that π Sco has $E_{B-V} = 0.08$ while that for HD31726 is only 0.05. (The factor 8.1 is the average value of $A_{1140Å-V}/E_{B-V}$ reported by Savage and Mathis[5].) The *Copernicus* and *IUE* values of 580 and 680 phot cm^{-2} s^{-1} Å^{-1}, respectively, were averaged to obtain a flux of 630 phot cm^{-2} s^{-1} Å^{-1} from π Sco. Since each 30μ pixel on the CCD subtends 0.00475Å at 1140Å, we find that the effective area of IMAPS (i.e., the product of the geometrical aperture area, instrument's optical efficiency and the detector's quantum efficiency) is 3.76 cm^2. This value is 2.5 times a lower limit for the efficiency we measured at

[3]Snow, T. P. and Jenkins, E. B. 1977, *Astrophysical Journal Supplement*, **33**, 269.
[4]*IUE Ultraviolet Spectral Atlas*, International Ultraviolet Explorer (IUE) NASA Newsletter no. 22 (Special Edition), p. 74.
[5]Savage, B. D. and Mathis J. S. 1979, *Annual Reviews of Astronomy and Astrophysics*, **17**, 73.

NRL before the flight[6], but only 0.61 times the figure of 6.14 cm^2 we calculated for the product of measured and expected efficiencies of the components in the instrument (249 cm^2 aperture $\times$ 0.74 unobscured portion of the beam through the collimator $\times$ 0.83 ratio of the principal [zero order] beam to the collimator's total throughput, including diffraction spikes $\times$ 0.25 efficiency measured for the echelle grating $\times$ 0.24 efficiency measured for the cross-disperser grating $\times$ 0.67 quantum efficiency usually obtained at this wavelength for a KBr photocathode on a solid substrate).

We suspect that the most probable reason for the actual efficiency being somewhat lower than expected was that the photocathode degraded slightly. In spite of our using our best efforts to keep the KBr away from any humidity during the installation of the photocathode, we think some exposure to slightly humid air may have occurred. At one point, the payload had to be opened to repair a suspicious connection on a plug associated with the detector electronics. This field repair was done at WSMR long after the photocathode was installed. It is also possible that the reflectivities of the gratings could have deteriorated slightly or that the real quantum efficiency of an ICCD is somewhat lower than that of the photocathode by itself (see §7 for a possible explanation of this effect, if it exists). Finally, it seems to be generally true that astronomers discover that an assembled instrument has an overall efficiency which seems to be noticeably lower than the product of the efficiency of the separate components, for reasons they seem never able to explain satisfactorily.

[6]When we exposed the IMAPS payload to a collimated beam from an argon discharge source, we found the effective area to be 1.5 cm^2. We knew at the time that this measurement was a lower limit for the sensitivity of IMAPS at 1048 and 1067Å because 1) The comparison monitor (a calibrated channeltron detector) also registered Lα and various emission lines from other impurities in the source, and 2) A significant percentage of the hits which were evident on the IMAPS frame were probably double events (they showed up with approximately twice the normal amplitude).

7. Laboratory Measurements of Quantum Efficiency

From 1983 to 1985, we collaborated with G. Carruthers at NRL to perform a series of special measurements to compare detective quantum efficiencies CsI-coated MCP detectors with CCD and MCP arrangements with separate, opaque photocathodes of the type discussed above. The opaque CsI photocathodes were used in either a Schmidt camera or an oblique-focussing electron-optical assembly. In addition to relating the photoefficiencies to the different detector configurations and studying variations with wavelength, we also wanted to compare the stabilities of the opaque and MCP-deposited CsI photocathode after exposure to different environmental conditions, such as high vacuum, partial vacuum, dry nitrogen and dry air.

The results of the research in quantum efficiencies were summarized in paper written by Carruthers and Opal [ref. 8] and Carruthers [ref. 10]. The latter paper is reproduced in Appendix C, since it relates all of the conclusions which evolved from the QE comparisons supported by this grant. Subsequent investigations were performed to determine whether or not the CCDs responded to all of the electrons emitted by the opaque photocathode. While there were some awkward sources of uncertainties in the measurements, they generally indicated that somewhat less than 100% of the electrons could be registered. This conclusion is consistent with the results of other investigators which indicated that the incident photoelectrons could be backscattered from the CCD. These results, based on using both RCA and TI CCDs, were written in a paper authored by Carruthers, Opal, Jenkins, Lowrance and Heckathorn which has been submitted for publication in the proceedings of the 1987 Imperial College Symposium on photoelectronic imaging devices [ref 11]. A copy of this paper is reproduced in Appendix D.

8. Microscopic Response of MAMA Detectors

In addition to quantum efficiency, an important feature of the opaque photocathode employed in our ICCD detector is the smoothness of response over very short length scales in the image. By contrast, for a detector which uses an MCP to sense the photoelectrons and provide the gain, this may not be true. In the course of deliberations on the properties of a large image sensor in the Starlab project[7], there was much concern expressed that the MCP detector in the instrument would respond to very small, point-like images in an irregular (and probably unpredictable) manner. In particular, when the size of the image approaches the inter-pore spacing on the MCP, the response would be modulated, and the photometric accuracy might be unacceptably low. This was suspected to be especially true if the photocathode were on the surface of the MCP itself, rather than on the back side of a window just in front of the MCP.

To test whether or not this possible small scale variation in quantum efficiency for MCP driven detectors was a valid concern, we cooperated with G. Timothy and J. Morgan at Stanford to measure the response of a MAMA detector when it was exposed to a slowly moving spot of light created by an all-reflective microscope. The microscope was operated in the reverse of the usual configuration; it created a small image of an illuminated pinhole. After special adjustments to compensate for spherical aberration in the faceplate of the detector, the microscope could produce a spot size of 3μ (FWHM) on the photocathode. A schematic diagram of the complete test facility is shown in Fig. 22.

Most of the effort supported by NSG-7618 was devoted to setting up the apparatus. Our grant paid for the purchase of the all-reflecting microscope, and we made use of the precision x-y-z stepper motor translation tables purchased earlier by Princeton for work done under grant NSG-5277. Considerable effort was expended to make the test facility versatile, stable

[7]Starlab was a proposed 1-meter, orbiting telescope to carry out wide field imagery to sub-arc second resolution in the ultraviolet and visible. It was also planned that this facility would have a long-slit echelle spectrograph. This study project was a joint enterprise of the United States, Canada and Australia. The project was abandoned when Canada withdrew.

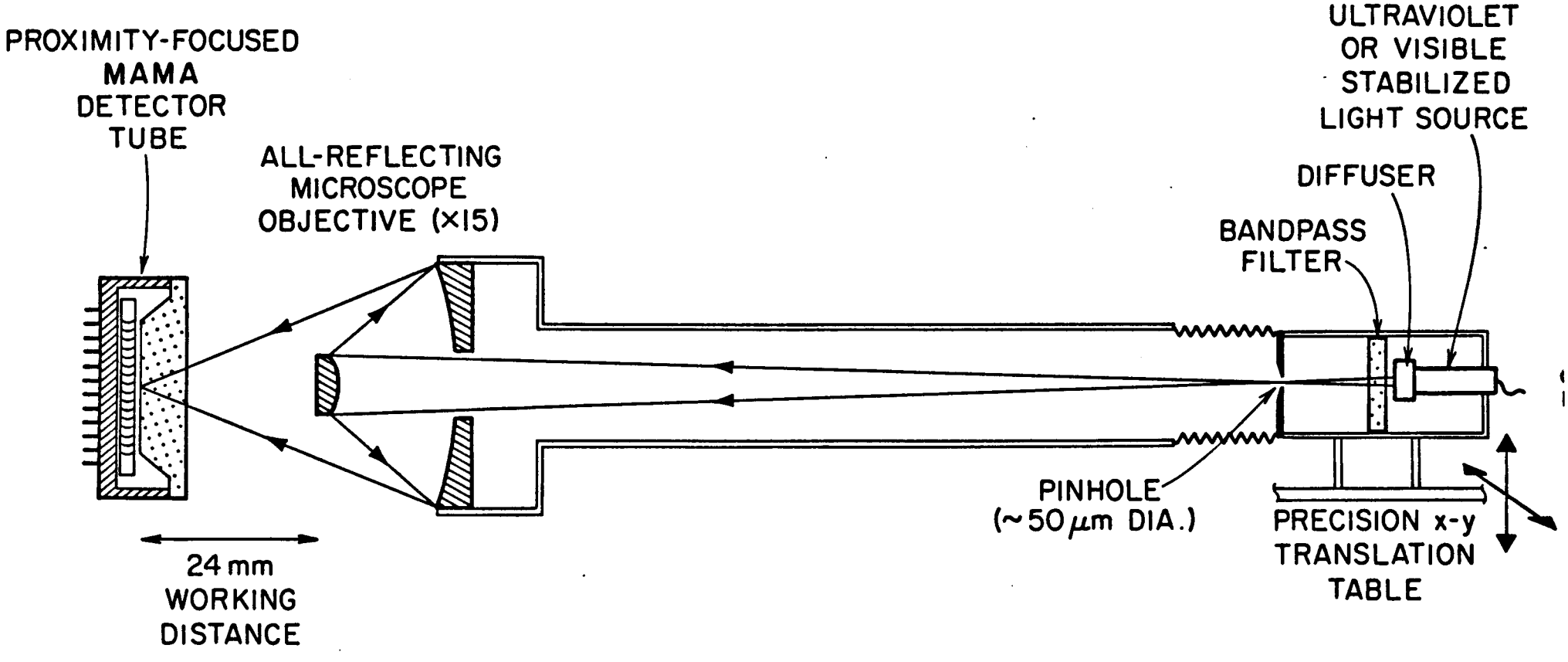

Figure 22. A schematic of the precision optical test facility created at Stanford to study the fine scale response of MAMA detector tubes.

and of high performance. Most of the test runs we executed during the grant period told us more about the limitations of the test apparatus, rather than fundamental properties of the detector's performance that we were interested in. Nevertheless, these ventures were crucial steps toward our ultimate goals, and we eventually were able to achieve the necessary precision when we overcame the problems.

Within the last month or so, our collaborators at Stanford have carried out some measurements of the response of a MAMA detector. As expected, there is considerable variation in the raw signal output from one position to the next on the MAMA. However, when one attempts to eliminate the ripple by dividing the result by a flat-field calibration frame, not all of the variations are removed, even though there is considerable improvement. The remaining peak-to-peak fluctuations are of order 20%. From the nature of the residual pattern, it appears that the variability is caused by changes in the collection efficiency of the anode structures.

The MAMA tube which was tested made use of the "course-fine" anode structure and logic system. The next generation of MAMA tubes will use the "fine-fine" system for position sensing of events, and we anticipate that the variations in response will much weaker. We have yet to show patterns which indicate a modulation caused by the pore structures in the MCP. A detailed discussion of the outcome will appear in an article which is about to be submitted to *Applied Optics* [ref. 13].

BIBLIOGRAPHY

(Publications Supported by NSG-7618)

1. "ICCD Development at Princeton" by J. L. Lowrance, P. Zucchino, G. Renda, and D. C. Long, *Advances in Electronics and Electron Physics,* **52**, 441 (1979).
2. "Intensified CCD Single Photoelectron Response" by J. L. Lowrance and P. Zucchino, *Instrumentation in Astronomy III, SPIE Proc.* **172**, 232 (1979).
3. "Light Emission from CCDs" by P. Zucchino, J. L. Lowrance, and J. Walker, *Applied Optics,* **19**, 2276 (1980).
4. "Electron Bombarded Charge Coupled Device (CCD) Detectors for the Vacuum Ultraviolet", by J. L. Lowrance and G. R. Carruthers, *Ultraviolet and Vacuum Ultraviolet Systems, SPIE Proc.* **279**, 123 (1981).
5. "Evaluation of RCA Thinned Buried Channel Charge-Coupled Devices (CCDs) for Scientific Applications", by P. Zucchino, D. Long. J. L. Lowrance, G. Renda, D. D. Crawshaw, and D. F. Battson, *Solid State Imagers for Astronomy, SPIE Proc.* **290**, 174 (1981).
6. "Echelle Spectroscopy with a Charge-Coupled Device (CCD)" by D. G. York, E. B. Jenkins, P. Zucchino, J. L. Lowrance, D. Long, and A. Songaila, *Solid State Imagers for Astronomy, SPIE Proc.* **290**, 202 (1981).
7. "Texas Instruments Virtual Phase CCD Imager Operated in the Frontside Electron-Bombarded Mode", by P. Everett, J. Hynecek, P. Zucchino, and J. L. Lowrance, *Instrumentation in Astronomy IV, SPIE Proc.* **331**, 151 (1982).
8. "Detection Efficiencies of Far-Ultraviolet Photon-Counting Detectors" by G. R. Carruthers and C. B. Opal, *Adv. Electronics and Electron Physics,* **64B**, 299 (1985).
9. "Oblique Magnetic Focus Point Spread Profiles and MTFs" by J. L. Lowrance, *Adv. Electronics and Electron Physics,* **64B**, 591 (1985).
10. "Quantum Efficiencies of Imaging Detectors with Alkali Halide Photocathodes. 1: Microchannel Plates with Separate and Integral CsI Photocathodes" by G. R. Carruthers, *Applied Optics,* **26**, 2925 (1987).
11. "Development of EBCCD Cameras for the Far Ultraviolet" by G. R. Carruthers, C. B. Opal, E. B. Jenkins, J. L. Lowrance, and H. M. Heckathorn, submitted for publication in the proceedings of the 9th Symposium on Photoelectronic Imaging Devices, Imperial College, 1987.
12. "An XUV Image Sensor for Rowland Circle Spectrographs" by J. L. Lowrance and C. L. Joseph, submitted for publication in the proceedings of the 9th Symposium on Photoelectronic Imaging Devices, Imperial College, 1987.
13. "Centroid Position Measurements with the MAMA Detector" by J. S. Morgan, D. C. Slater, J. G. Timothy, and E. B. Jenkins, to be submitted to *Applied Optics.*

APPENDIX A

A Method of Solution for the Most Probable Position of a Photoelectron Impact

Assume the secondary electrons to have a surface distribution

$$n = \frac{N}{w^2\pi} \exp\left[\frac{-(x - x_0)^2 - (y - y_0)^2}{w^2}\right] \tag{1}$$

where N is the total number of electrons and the unit of length for x, y and w is the dimension of a pixel. A determination of the most probable x_0 and y_0 may be defined as the combination which gives closest match of n integrated over the different pixel areas to the respective signal amplitudes which were recorded. Least squares solutions for x_0 and y_0 may be evaluated independently since n, as defined above, may be factored into x and y dependent functions.

If we isolate the pixel with the largest signal (pixel 5 shown below) and its nearest neighbors, we have for a given x_0 an expected signal fraction summed over pixels 1, 4 and 7

$$E_1 = \frac{1}{w\sqrt{\pi}} \int_{x_0}^{\infty} \exp(-x^2/w^2)\,dx \tag{2}$$

and in pixels 3, 6 and 9

$$E_2 = \frac{1}{w\sqrt{\pi}} \int_{1-x_0}^{\infty} \exp(-x^2/w^2)\,dx \tag{3}$$

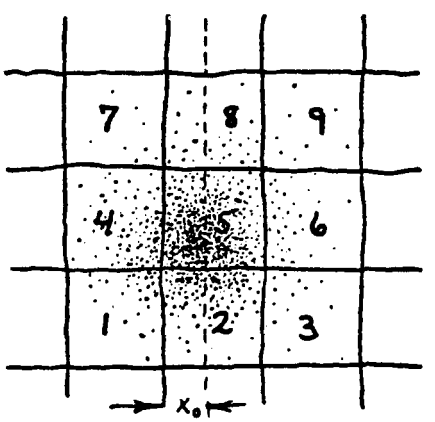

(Strictly speaking, the upper limits for the integrals in equations (2) and (3) should be $1 + x_0$ and $2 - x_0$, respectively, but for values of w which seem practical the infinite limits are accurate enough.) To solve for the best x_0 we evaluate

$$\sum_{i=1}^{2} (E_i - f_i) \frac{\partial E_i}{\partial x_0} = 0 \tag{4}$$

where the f_i are the observed fractions of the total signals falling in the domains of the respective E_i. Since

$$\frac{\partial E_1}{\partial x_0} = -\frac{1}{w\sqrt{\pi}} \exp\ (-x_0^2/w^2) \tag{5}$$

and

$$\frac{\partial E_2}{\partial x_0} = \frac{1}{w\sqrt{\pi}} \exp\left[-\frac{(1 - x_0)^2}{w^2}\right] \tag{6}$$

we may substitute equations (5) and (6) into equation (4) and factor out $2/w\sqrt{\pi}\ \exp(-x_0^2/w^2)$ to obtain the equation

$$-\frac{1}{w\sqrt{\pi}} \int_{x_0}^{\infty} \exp(-x^2/w^2)\,dx + f_1 + \left[\frac{1}{w\sqrt{\pi}} \int_{1-x_0}^{\infty} \exp(-x^2/w^2)\,dx - f_2\right] \exp\left(\frac{2x_0 - 1}{w^2}\right) = 0 \tag{7}$$

An identical analysis is performed for y_0 substituting pixels 1, 2 and 3 for domain 1 and 7, 8 and 9 for domain 2.

In actual application, equation (7) will be solved for all possible values of f_1 and f_2 to generate a two-dimensional lookup table. This table may then be used in the real-time data processing to establish rapidly the positions of

events. This procedure was followed to generate the data shown in Figure 3: the table contained 120 × 120 values representing $0 < f_i < 1.2$ in steps of 0.01, and the computer selected entries which were closest to the measured f_i.

APPENDIX B

A Method for Determining the Profile of the ICCD Electron Distribution

We irradiate the photocathode with a reasonably uniform illumination and run the electron optics in a very out-of-focus condition to make the distribution of photoelectron events on the CCD as uniform as possible. We then assume

1) The positions of events are purely random
2) The distribution has circular symmetry
3) The distributions have no significant variability from one event to the next.

Assumption (3) must be verified in the analysis of events. A small variability will be measurable but should not have very serious consequences on the basic determinations of the average shape of the distribution.

For each photoelectron event we integrate the secondary electron signals deposited over short segments along adjacent lines of pixels. These segments should be just long enough to include the entire distribution along a line; including too many pixels will unnecessarily raise the noise. These signals are re-expressed as fractions f of the total charge and stored for many events, to be subsequently used for constructing a frequency distribution P(f). For an event located at a distance y_0 from a line center, we would expect to register a signal whose behavior with position follows the relationship

$$F(y_0) = \int_{-0.5}^{0.5} \int_{-\infty}^{\infty} n(x, y - y_0)\,dxdy \Big/ \int_{-\infty}^{\infty} \int_{-\infty}^{\infty} n(x, y)\,dxdy$$

for a surface distribution of electrons $n(x - x_0, y - y_0)$ of an event centered on x_0, y_0. If the events are distributed uniformly over all y_0 we have $P(f) = |dF/dy_0|^{-1}$. Thus, after measuring P(f) one may determine $F(y_0)$ by evaluating its

reciprocal $G(f) = \int_0^f P(f')df'$. In the analysis, we must allow for the fact that noise in the data will smooth P(f) somewhat. The apparent P(f) is the true P(f) convolved with a Gaussian profile whose width corresponds to the rms noise in the line divided by the total signal. The function n(x,y) may be extracted from $F(y_0)$ by standard deconvolution techniques.

As an example, we may consider a circular Gaussian distribution n(x,y) defined by equation (1) of Appendix A. Figure 8 shows P(f) and $F(y_0)$ for five different widths.

A test of assumption (3) may be accomplished by studying how well the signal fractions in different lines for a single event conform to the average $F(y_0)$ at points spaced one unit apart in y.

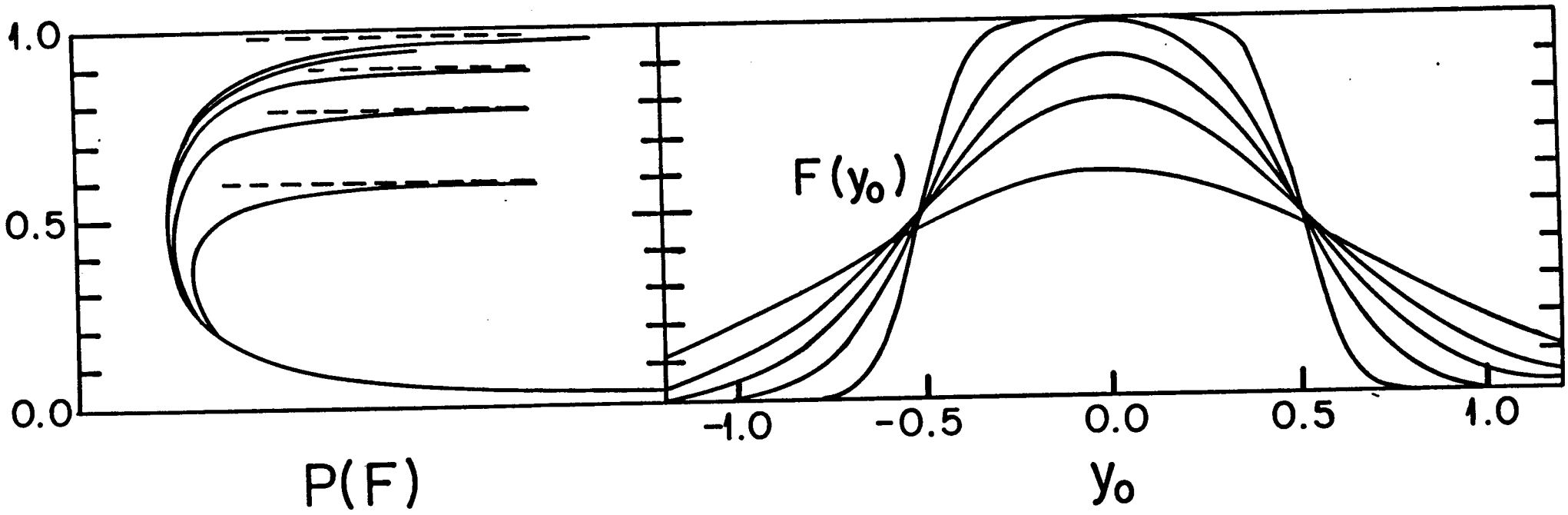

Fig. 8 - Plots of $F(y_0)$ as a function of y_0 (right) and P(F) (left) for five different widths of the Gaussian spread function for secondary electrons.